

iPSC modeling of young-onset Parkinson's disease reveals a molecular signature of disease and novel therapeutic candidates

A. H. Laperle^{1,10}, S. Sances^{1,10}, N. Yucer^{1,10}, V. J. Dardov¹, V. J. Garcia¹, R. Ho¹, A. N. Fulton¹, M. R. Jones^{2,3}, K. M. Roxas¹, P. Avalos¹, D. West¹, M. G. Banuelos¹, Z. Shu⁴, R. Murali^{5,6,7}, N. T. Maidment⁴, J. E. Van Eyk^{2,7,8}, M. Tagliati⁹ and C. N. Svendsen^{1*}

Young-onset Parkinson's disease (YOPD), defined by onset at <50 years, accounts for approximately 10% of all Parkinson's disease cases and, while some cases are associated with known genetic mutations, most are not. Here induced pluripotent stem cells were generated from control individuals and from patients with YOPD with no known mutations. Following differentiation into cultures containing dopamine neurons, induced pluripotent stem cells from patients with YOPD showed increased accumulation of soluble α -synuclein protein and phosphorylated protein kinase C α , as well as reduced abundance of lysosomal membrane proteins such as LAMP1. Testing activators of lysosomal function showed that specific phorbol esters, such as PEPO05, reduced α -synuclein and phosphorylated protein kinase C α levels while increasing LAMP1 abundance. Interestingly, the reduction in α -synuclein occurred through proteasomal degradation. PEPO05 delivery to mouse striatum also decreased α -synuclein production in vivo. Induced pluripotent stem cell-derived dopaminergic cultures reveal a signature in patients with YOPD who have no known Parkinson's disease-related mutations, suggesting that there might be other genetic contributions to this disorder. This signature was normalized by specific phorbol esters, making them promising therapeutic candidates.

Parkinson's disease (PD) is a movement disorder that can be caused by monogenic mutations in specific genes (<10% of cases) or a poorly understood combination of environmental and genetic factors^{1,2}. The pathological hallmarks of PD include progressive loss of nigral dopamine neurons and Lewy bodies, which are cytoplasmic inclusions containing abnormally aggregated α -synuclein protein³. Native-state α -synuclein, localized to presynaptic terminals, functions in vesicle trafficking and neurotransmitter release and reuptake⁴. Mutations or triplication of the α -synuclein gene (*SNCA*) are rare but can cause PD, suggesting that simple overexpression of this protein is critical to disease initiation and progression⁵.

The inaccessibility of patient dopamine neurons and poor animal models have hindered disease studies and effective drug discovery. Reprogramming patient-derived cells into induced pluripotent stem cells (iPSCs) with subsequent differentiation into dopamine neurons provides a human tissue-specific model of PD⁶. As reprogramming removes most of the epigenetic changes, disease-specific phenotypes originate from the patient's genetic composition and represent the very earliest stages of the disease process^{7,8}.

Patient iPSCs harboring monogenic PD mutations have been used to elucidate the role of α -synuclein in the origin and progression of PD^{9–17}. While iPSC-derived dopaminergic cultures with monogenic mutations display phenotypic abnormalities and α -synuclein accumulation^{14,15}, inherited PD represents <10% of

cases. However, iPSC models of the prevalent sporadic form of PD do not show α -synuclein accumulation compared to controls^{10,15}.

Ten percent of patients with PD have YOPD, defined as a diagnosis between 21 and 50 years of age^{18–20}. Over 80% of these patients have no familial history or known PD mutations²¹. It is likely that early onset of disease may produce a more severe phenotype in iPSC models, as seen for early-onset diseases such as spinal muscular atrophy²². We therefore generated iPSC lines from control individuals and patients with YOPD with no known PD mutations and explored disease-specific phenotypes.

Results

Generation of iPSCs from patients with YOPD. We collected peripheral blood mononuclear cells from three patients with YOPD (aged 30–39 years) with no known familial history of PD or PD mutations (Supplementary Table 1; 190iPD, 194iPD and 200iPD). Cells were reprogrammed with nonintegrating episomal techniques to iPSC lines, which expressed pluripotency markers and were karyotypically normal (Extended Data Fig. 1a,b). Analysis with the NeuroX platform²³ and whole-genome sequencing (WGS) detected no causal monogenic mutations in the established PD genes *EIFG1*, *PARK2*, *LRRK2*, *GBA*, *SNCA*, *PINK1*, *PARK7*, *VSP35* and *ATP13A2* or amplifications of the *SNCA* locus (data not shown and Supplementary Table 2a,b)¹. Polygenic risk scores based on WGS indicated that patients with YOPD harbored

¹Cedars-Sinai Board of Governors Regenerative Medicine Institute, Los Angeles, CA, USA. ²Department of Biomedical Sciences, Cedars-Sinai Medical Center, Los Angeles, CA, USA. ³Center for Bioinformatics and Functional Genomics, Cedars-Sinai Medical Center, Los Angeles, CA, USA. ⁴Department of Psychiatry and Biobehavioral Sciences, Semel Institute for Neuroscience and Human Behavior, University of California, Los Angeles, CA, USA. ⁵Samuel Oschin Comprehensive Cancer Institute, Los Angeles, CA, USA. ⁶Research Division of Immunology, Cedars-Sinai Medical Center, Los Angeles, CA, USA. ⁷Department of Medicine, Cedars-Sinai Medical Center, Los Angeles, CA, USA. ⁸Smidt Heart Institute, Cedars-Sinai Medical Center, Los Angeles, CA, USA. ⁹Department of Neurology, Cedars-Sinai Medical Center, Los Angeles, CA, USA. ¹⁰These authors contributed equally: A. H. Laperle, S. Sances, N. Yucer.

*e-mail: clive.svendsen@cshs.org

a subset of genome-wide association-identified PD risk alleles²⁴ (Supplementary Table 2a). Patients displayed diverse PD phenotypes and all had asymmetric onset with multiple tests to confirm diagnosis (Supplementary Table 1). Three control iPSC lines were generated from the blood or fibroblasts of individuals with no neurological disease at the time of sample collection (Supplementary Table 1; 02iCTR, WP3iCTR and 00iCTR).

Differentiation of iPSCs to midbrain dopaminergic cultures.

iPSC lines from patients with YOPD and controls were differentiated to midbrain dopaminergic (mDA) neural cultures using a modified 30-d protocol²⁵ (Fig. 1a). Differentiated cultures expressed neural markers (*PAX6* and *NEFH*), neuronal markers (*TUB3* and *MAP2*) and, notably, dopaminergic neuron markers, including tyrosine hydroxylase (*TH*), *FOXA2*, *Nurr1*, *DAT* and *GIRK2* (Extended Data Fig. 2a)^{25–27}. Immunostaining and flow cytometry quantification showed TH production and similar numbers of TH-expressing cells for control and YOPD lines (Fig. 1b,c). While the 190iPD and 02iCTR lines had significantly different expression, no other inter-line differences were significant. Following normalization of TH-expressing neuron numbers, high-performance liquid chromatography (HPLC) analysis demonstrated that all lines produced and released similar amounts of dopamine (Fig. 1d and Extended Data Fig. 2b,c). To determine the electrophysiological function of mDA cultures, patch-clamp and multielectrode array (MEA) recordings were conducted over time in culture. Spontaneous activity was observed at day 21 of differentiation (Extended Data Fig. 2d) and, by day 30, YOPD and control cells produced coordinated bursts of activity (Extended Data Fig. 2e). Quantification across lines showed similar numbers of spontaneous spikes in disease and control cultures (Extended Data Fig. 2f). Neurons patched at day 30 exhibited spontaneous activity (Fig. 1e) with large voltage-gated sodium and potassium currents (Fig. 1f) and elicited trains of action potentials upon current injection (Fig. 1g), indicative of mature neurons. Patched PD and control neurons exhibited similar capacitance, resting membrane potential, inward rectifying potassium current and delayed rectifying potassium current (Extended Data Fig. 3a–e), although YOPD neurons had a reduced sodium current. These data demonstrate that YOPD-derived iPSCs differentiated efficiently into functional dopaminergic neurons and possessed similar neuronal profiles to controls.

α -synuclein accumulates specifically in YOPD mDA cultures.

We next determined whether α -synuclein was differentially expressed in YOPD-derived mDA cultures. qPCR showed that *SNCA* gene expression was not significantly increased in YOPD mDA cultures relative to controls (Fig. 1h). Conversely, both western blot and ELISA analyses showed that YOPD mDA cultures had significantly increased α -synuclein protein levels (Fig. 1i,j), and analysis of soluble and insoluble lysates demonstrated a lack of synuclein multimers (Extended Data Fig. 4). YOPD lines did not accumulate α -synuclein at the iPSC stage, indicating specificity to differentiated cultures (Extended Data Fig. 5a,b). Collectively, these data show that mDA cultures demonstrate a YOPD phenotype of transcription-independent α -synuclein protein accumulation.

Lysosomal proteins are dysregulated in YOPD mDA cultures.

We next examined what factors might contribute to increased levels of α -synuclein protein. Using a paired-sample set derived from the same culture wells, whole-transcriptomic RNA sequencing (RNA-seq) detected 19,004 unique transcripts in comparison of YOPD and control lines (Extended Data Fig. 6a), while data-independent-acquisition mass spectrometry (SWATH) proteomic analysis identified 2,478 unique proteins (Extended Data Fig. 6b,c). Independent unsupervised principal-component analyses (PCA) of both transcriptomic and proteomic data revealed a clear delineation

between the YOPD and control cells along principal component 1 (PC1; Fig. 2a).

Given the similarity between the transcriptomic and protein signatures, we compared the two datasets along PC1 to identify both concordant and discordant cellular pathways that could contribute to α -synuclein accumulation. To enable direct comparison of pathways, PCA was repeated on 2,440 genes and corresponding proteins that were present in both datasets (Extended Data Fig. 6d,e). PC1 ranked genes and proteins from the matched list were analyzed in separate gene-set enrichment analyses (GSEAs) and compared by term significance (Fig. 2b). GSEA on the entire RNA-seq dataset yielded similar significant terms (Supplementary Table 3). The genes encoding α -synuclein and other synaptic vesicle proteins related to dopamine release, such as synapsin (*SYP*), synaptic vesicle 2A (*SV2A*) and *SNAP25*, were in the GO_Presynapse term, which was significantly upregulated in both the RNA and protein datasets (Fig. 2b). Protein terms related to PD, Alzheimer's disease and Huntington's disease were significantly upregulated in YOPD lines, suggesting capture of common aspects of neurodegeneration.

Transcripts and proteins found in the GO_Endoplasmic_Reticulum_Lumen term were significantly downregulated, suggesting deficiencies in genes related to proteogenesis. Interestingly, lysosomal genes in the GO_Lysosomal_Lumen term were significantly downregulated at the protein but not the mRNA level (Fig. 2b, black arrow). To demonstrate that significance for these lysosomal and endoplasmic reticulum (ER) terms was not driven by the outlying 190iPD line, paired analysis was repeated without the 190iPD line and results again showed that lysosomal and ER lumen proteins corresponded to prominently dysregulated pathways (Extended Data Fig. 6f,g). In contrast, when the 190iPD line was removed from analysis, significant mRNA and protein upregulation was lost for genes belonging to mitochondria-related terms (KEGG_Oxidative_Phosphorylation, GO_Mitochondrial_Respiratory_Chain_Complex_1_Biogenesis and GO_Mitochondrial_Membrane_Part) and GO_Dopaminergic_Neuron_Differentiation. These results indicate that, while differences in these terms were driven entirely by the 190iPD line, lysosomal pathway changes were present across the cohort. To further confirm YOPD specificity for the dysregulated pathways found in PC1, differential expression between control and YOPD lines was analyzed with proteomic data and differentially expressed proteins were entered into STRING pathway analysis (Fig. 2d). Lysosomal proteins again had significantly reduced levels in YOPD lines (Fig. 2e). These data indicate that, while YOPD mDA cultures had normal transcription of lysosomal machinery, less resulting protein was present compared to controls.

The reduced amounts of lysosomal proteins suggested that impaired protein degradation could underlie α -synuclein accumulation. To test overall degradation rates, global transcriptional function was inhibited for 48 h via cycloheximide treatment and protein was quantified over time (Fig. 3a,b). α -Synuclein was degraded in the 02iCTR line with a half-life of approximately 10 h, slightly longer than the half-life previously reported in PC12 cells²⁸. In stark contrast, α -synuclein accumulated in the line derived from the most severe case of PD (190iPD) over the course of cycloheximide treatment. However, disease-derived and control lines displayed similar degradation rates for other proteins relevant to dopamine neurons, such as TH and synaptophysin (Fig. 3b), suggesting that the deficit was specific to α -synuclein.

Protein degradation can largely be divided into proteasomal and autophagy and lysosomal pathways. To determine whether proteasomal degradation was responsible for α -synuclein proteolysis^{28,29}, mDA cultures were treated with the proteasome inhibitor MG132 for 24 h. This resulted in accumulation of p53, a protein canonically degraded via proteasomal means (Fig. 3c,d). However, the amount of α -synuclein in control and YOPD cultures was not significantly increased (Fig. 3e), indicating that α -synuclein degrada-

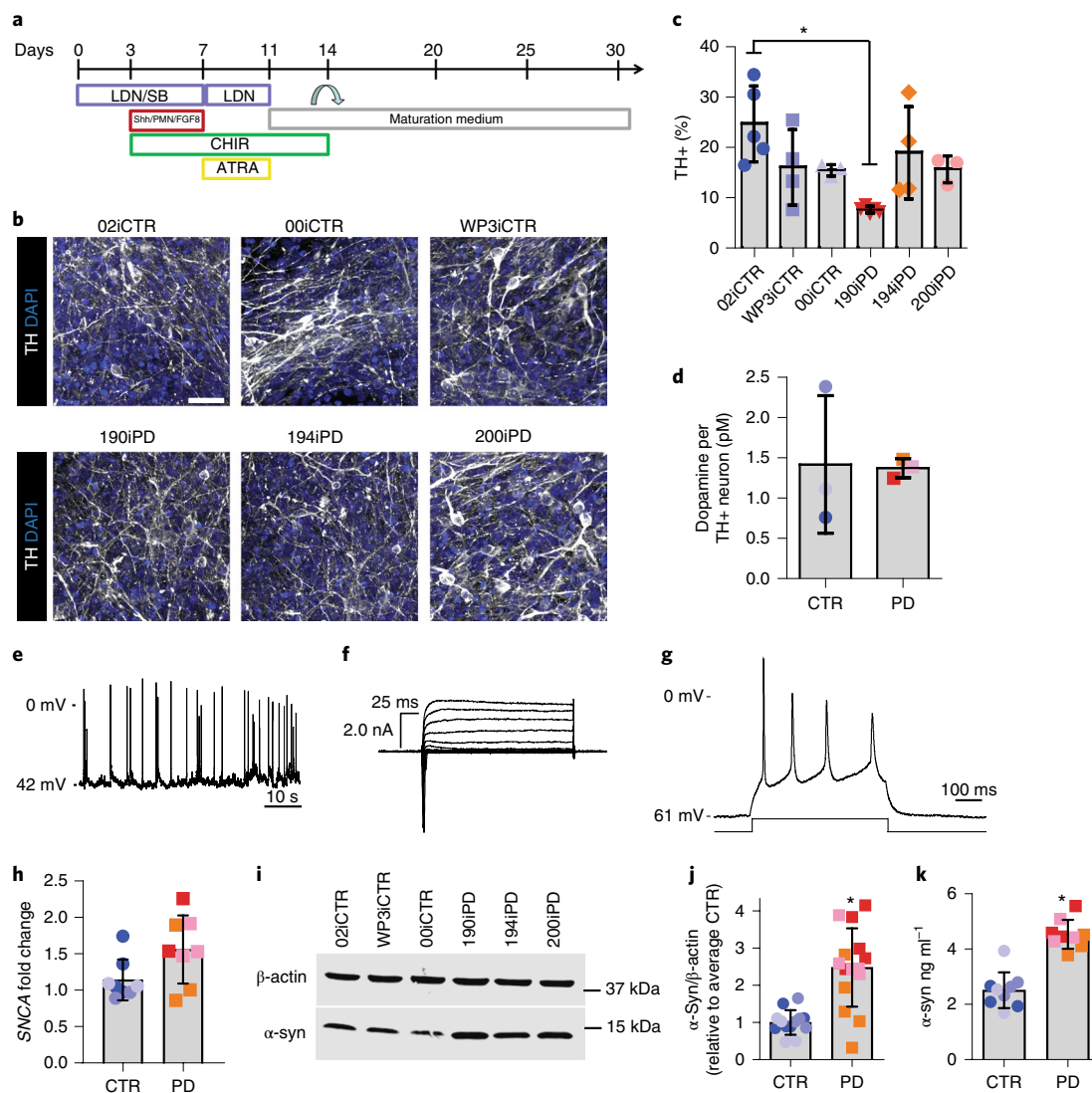


Fig. 1 | YOPD-derived iPSCs can be differentiated into mDA neural cultures that accumulate α -synuclein. **a**, Differentiation schematic for mDA cultures. **b**, Representative images of mDA cultures showing TH expression and morphology. Similar results were observed across four independent studies. **c**, Flow cytometry quantification of differentiation efficiency, with each point representing an average of three separate wells of an independent experiment (02iCTR, $n=5$ independent experiments; WP3iCTR, $n=4$; 00iCTR, $n=3$; 190iPD, $n=5$; 194iPD, $n=4$; 200iPD, $n=3$). $*P=0.012$ by one-way ANOVA ($F=4.07$, $d.f.=23$) with Tukey multiple-comparisons test. **d**, HPLC detection of total dopamine content normalized to differentiation efficiency by line. Each point represents the average of three technical replicates per line. All samples were from the same differentiation with three control lines and three YOPD lines. **e**, Gap-free recordings of spontaneous activity in day 30 mDA neurons (8 of 29 patched cells had spontaneous activity). **f**, Voltage-clamp recordings of day 30 mDA neurons (all 29 patched cells had sodium and potassium currents under voltage-clamp). **g**, Injected current recordings of day 30 mDA neurons (23 of 29 patched cells fired action potentials on injection of current). **h**, SNCA expression by qPCR in day 30 mDA cultures. Each point represents an average of three biological replicates (wells) for one line from an independent differentiation. CTR, $n=8$; PD, $n=8$; $P=0.052$ by two-tailed Student's t -test with Welch's correction. **i**, Western blots of day 30 mDA cultures for α -synuclein production and β -actin as a housekeeping control. **j**, Relative intensities from multiple western blots (CTR, $n=13$; PD, $n=15$) with each point representing the band intensity from a separate differentiation; intensities are given relative to the average for the control lines. **k**, α -synuclein ELISA, with each point representing the average of three independent wells from a separate differentiation; three independent differentiations are represented for each line (CTR, $n=9$; PD, $n=9$). Colors on graphs indicate different iPSC lines. $*P<0.0001$ by two-tailed Student's t -test with Welch's correction in **j** and **k**. Bar graphs show the mean \pm s.d.

tion was not mediated by the proteasome in this context. Because MG132 lacks specificity as a proteasomal inhibitor, YOPD and control mDA cultures were treated with the more selective proteasomal inhibitors lactacystin and epoxomicin. Treatment with these inhibitors led to accumulation of p53 but not α -synuclein protein (Extended Data Fig. 7a–c), confirming our initial conclusion that α -synuclein is not degraded by proteasomal means in mDA cells. To determine lysosomal involvement in α -synuclein degradation^{30,31}, we probed for lysosomal-associated membrane protein 1

(LAMP1) and discovered that its levels were significantly reduced in all three YOPD lines, consistent with the proteomics analysis (Figs. 2e and 3f,g). Quantification of GCCase, a lysosomal hydrolase associated with PD^{32,33}, showed significant reduction of activity in YOPD mDA cultures (Fig. 3h). In a study using iPSC-derived neural cultures from patients with normal-onset PD, reduced GCCase activity was caused by an increase in oxidized dopamine at later culture time points (>60 d)³⁴. In contrast, YOPD cultures at 30 d did not show increased amounts of oxidized dopamine (Fig. 3i); however,

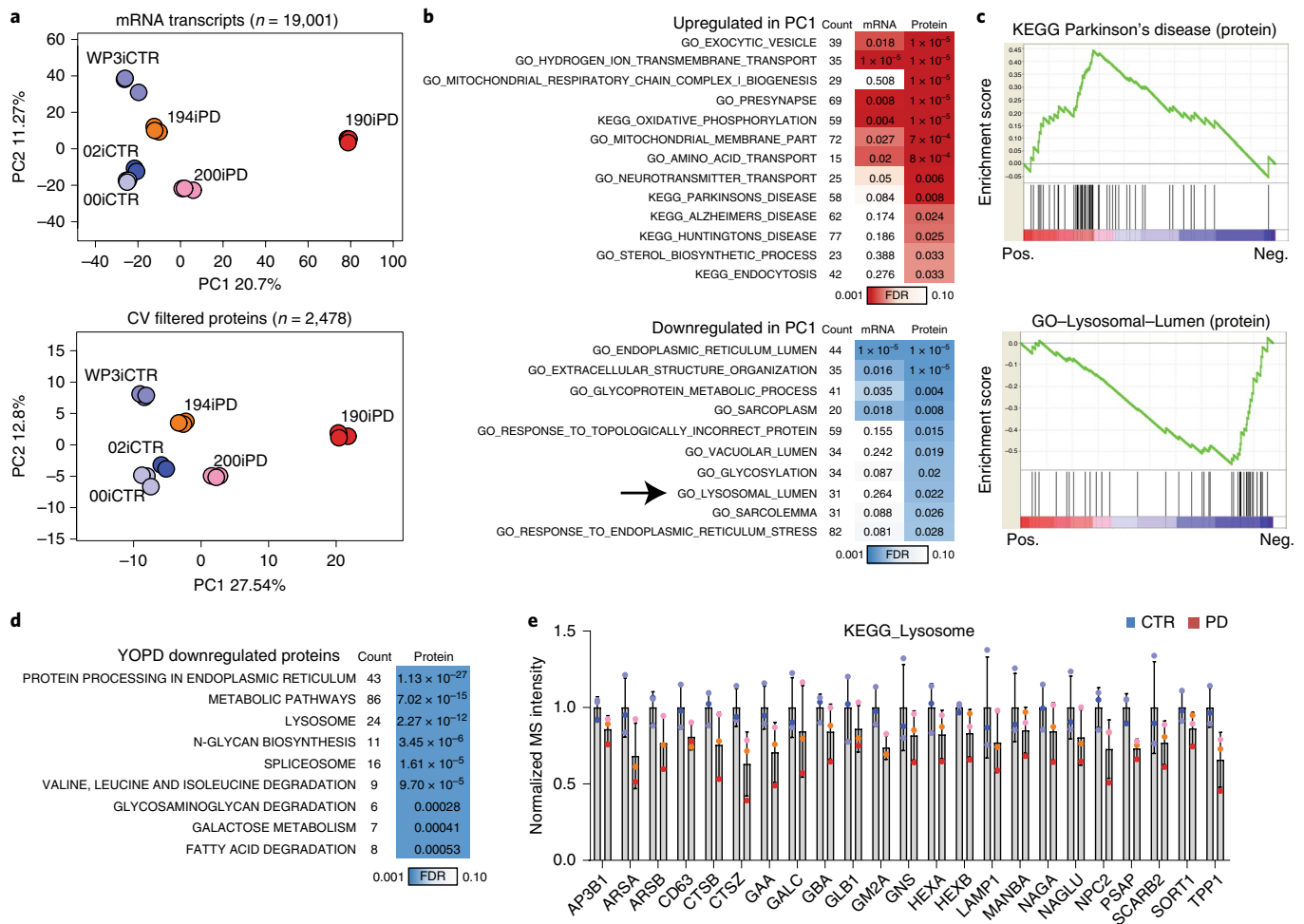


Fig. 2 | Paired RNA-seq and proteomic analyses from mDA cultures. a, PCA plots of whole-transcriptomic and CV-filtered proteomic datasets from matching mDA cultures at 30 d. Colors indicate cell lines: light blue, 02iCTR; dark blue, WP3iCTR; purple, 00iCTR; orange, 194iPD; pink, 200iPD; red, 190iPD. Replicate colors indicate biological replicates from different culture wells. **b**, GSEAs of matching gene set components upregulated and downregulated along PC1 from both RNA-seq and proteomic data. Pathways are ranked by significance ($P < 0.05$) calculated by FDR. Zero values in GSEA were set to 1×10^{-5} . **c**, Enrichment plots from proteomic analysis of GSEA terms significantly upregulated and downregulated in PC1: red, positive weighting score; blue, negative weighting score. Genes in PC1 are ordered by gene weighting along the x axis, and black lines indicate genes contained in a GSEA term. **d**, STRING analysis of differentially downregulated protein KEGG pathways. **e**, Average detected protein intensity values for significantly downregulated genes in the KEGG_Lysosome pathway. Colors indicate the average of each cell line. For all omics experiments, $n = 3$ independent biological replicates per line. Bar graphs show the mean \pm s.e.m.

oxidized dopamine began to accumulate in the YOPD cultures when cells were grown for longer time periods (60 d; Fig. 3j). These results suggest that increased α -synuclein and lysosomal deficiencies precede accumulation of oxidized dopamine, providing further evidence of dysfunctional lysosomal degradation as the putative cause of α -synuclein accumulation in YOPD mDA cultures.

PEP005 modulates YOPD phenotypes. We next attempted to reduce α -synuclein levels through activation of lysosomal-specific pathways using three lysosomal agonists³⁵: PEP005, a protein kinase C (PKC) agonist and structural analog of the HEP14 drug³⁶; SMER28, a small-molecule autophagy promoter that reduces Huntingtin and α -synuclein aggregates in PC12 cells³⁷; and trehalose, another compound that promotes α -synuclein clearance in PC12 cells³⁸. mDA cultures from the 02iCTR and 190iPD lines were treated with each agonist for 3 d starting at day 27 of differentiation. Interestingly, treatment with PEP005 and SMER28, but not trehalose, reduced α -synuclein protein levels in controls (Fig. 4a,b). In YOPD cultures, PEP005 and trehalose, but not SMER28, reduced α -synuclein levels. However, only PEP005 reduced α -synuclein levels in both

control and YOPD cultures and, surprisingly, PEP005 also caused an increase in TH levels (Fig. 4a,b). Immunostaining confirmed decreased α -synuclein and enhanced TH levels (Extended Data Fig. 8a). The high density of TH immunostaining precluded quantification; however, flow cytometry confirmed that PEP005-treated cultures contained neurons with significantly more TH production (Fig. 4c), although the percentage of TH neurons was not increased (Fig. 4d). This suggests that levels were enhanced in neurons already producing the enzyme.

PEP005 has well-established activity against both PKC α and PKC δ . We were surprised to find that, at day 30, basal levels of phosphorylated PKC α (p-PKC α) were higher in 190iPD mDA cultures than in controls and that PEP005 treatment could completely ablate the signal in both control and YOPD cultures (Fig. 4a). Assessment of all other lines used in this study confirmed that there were higher p-PKC α levels in mDA cultures from all three YOPD lines than in controls (Fig. 4i,k), although differences in total PKC α levels were not significant (Fig. 4i,j). Elevated p-PKC α levels were absent in the undifferentiated iPSCs (Extended Data Fig. 5a,b) and no clear pattern was evident in peripheral blood from the individual patients

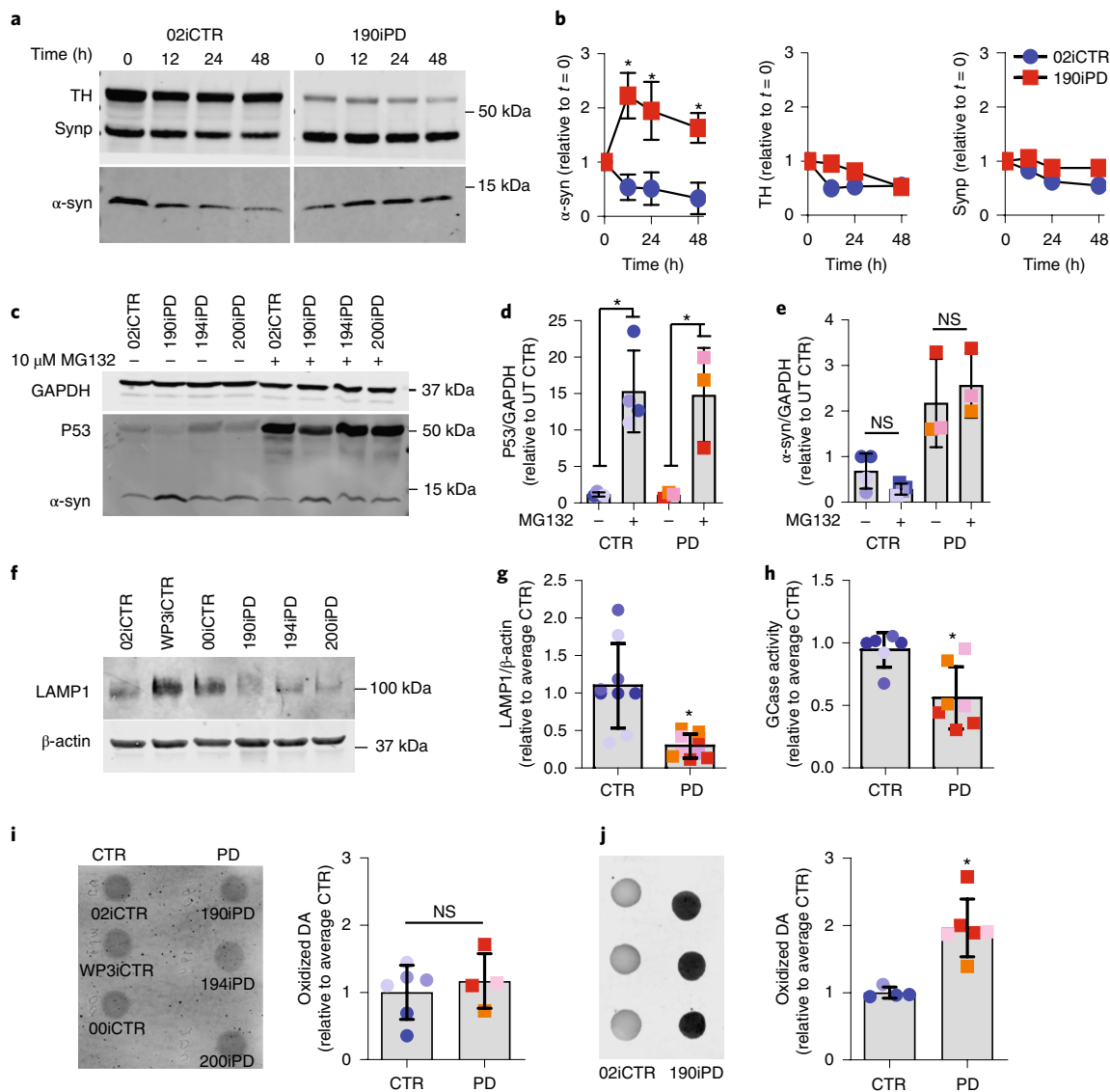


Fig. 3 | Lysosomal α -synuclein degradation is specifically impaired in YOPD mDA cultures. **a**, Representative western blots showing TH, synaptophysin (synp) and α -synuclein (α -syn) degradation under cycloheximide inhibition. **b**, Average intensities of three separate differentiations and western blots from the O2iCTR and 190iPD lines, presented as fold change relative to time 0. * $P < 0.0001$ compared to control cells at the same time point by one-way ANOVA ($F = 15.6$, d.f. = 23) with Sidak's multiple-comparisons test. **c**, Western blot showing α -synuclein degradation under 24 h of treatment with MG132 proteasomal inhibitor. Blots were quantified from multiple differentiations (CTR, $n = 4$; PD, $n = 3$), with each point representing the band intensity from a separate differentiation. **d,e**, Changes in band intensity after MG132 treatment for p53 ($F = 12.73$, d.f. = 13, $P = 0.004$ for CTR, $P = 0.012$ for PD) (**d**) and α -synuclein ($F = 12.53$, d.f. = 13, $P = 0.77$ for CTR, $P = 0.84$ for PD) (**e**) analyzed by one-way ANOVA with Tukey multiple-comparisons test relative to untreated cells. An asterisk indicates significance relative to untreated cells. **f**, Western blot showing LAMP1 protein in YOPD and control mDA cultures. **g**, Quantification of LAMP1 band intensity relative to control cells. Each point represents a separate differentiation and western blot (CTR, $n = 9$; PD, $n = 9$). * $P = 0.002$ compared to the average for control bands determined by two-tailed t -test with Welch's correction. **h**, For GCCase activity, two or three biological replicates (separate differentiations) were performed for each line, and each differentiation was measured in three technical replicates (three separate wells of the GCCase assay). The three technical replicates for each differentiation were averaged to present a single point on the graph for each separate differentiation. Data were normalized to control cells for each differentiation and are presented as the fold change (CTR, $n = 9$; PD, $n = 10$). * $P = 0.006$ relative to untreated cells by two-tailed t -test with Welch's correction. **i,j**, NIRF detection of oxidized dopamine in lysates from mDA cultures at day 30 (CTR, $n = 6$; PD, $n = 4$; $P = 0.54$) (**i**) and day 60 (CTR, $n = 4$; PD, $n = 6$; $P = 0.002$) (**j**). Dot blots and signal intensity relative to control cells are presented. An asterisk indicates significance relative to control cells determined via two-tailed t -test with Welch's correction. Bar graphs show the mean \pm s.d.

(data not shown), indicating specificity to the differentiated mDA cultures. Elevated p-PKC α levels were ablated by the addition of 1 μ M PEP005 for 3 d in mDA cultures from all iPSC lines (Fig. 4e,g), which was coupled with decreased α -synuclein (Fig. 4f) and increased LAMP1 (Fig. 4h) levels.

To further evaluate the response to PEP005, we treated mDA cultures over time. Within approximately 24 h, p-PKC α and

α -synuclein were degraded (Extended Data Fig. 8d,e) and there was a marked increase in TH levels, although LAMP1 protein levels were not altered (Extended Data Fig. 8d,e). LC3 I and LC3 II levels remained unchanged (Extended Data Fig. 8b,c), demonstrating that bulk autophagy is not altered by PEP005 within the first 24 h and therefore suggesting that bulk autophagy is not involved in PEP005-induced α -synuclein reduction. Gene expression data from paired

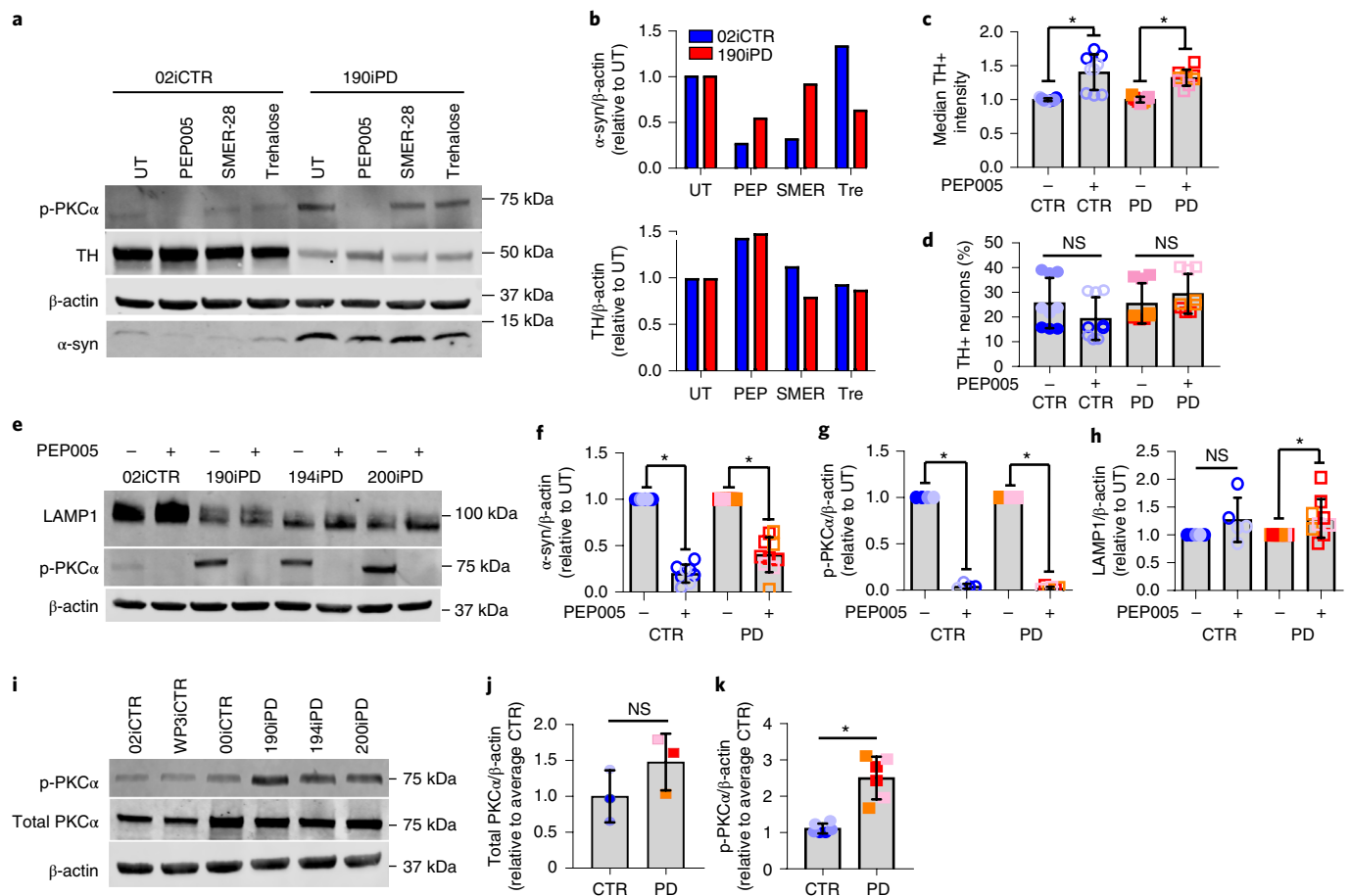


Fig. 4 | Treatment of YOPD mDA cultures with a PKC agonist reduces intracellular α -synuclein levels. **a,b**, Western blots (**a**) and relative band quantification (**b**) of day 30 mDA cultures from one experiment where cultures were left untreated (UT) or were treated with the indicated compound for 72 h. **c**, Flow cytometry analysis of day 30 mDA cultures treated with PEP005 for 72 h (CTR, $n=9$; PD, $n=9$) for the median TH intensity of TH-positive cells relative to untreated mDA cultures of the same line. An asterisk indicates a significant difference from the untreated culture determined by one-way ANOVA ($F=8.4$, $d.f.=35$, $P<0.0001$) with Sidak's multiple-comparisons test. **d**, Efficiency of differentiation into TH-positive neurons. Significance was determined by one-way ANOVA ($F=2.02$, $d.f.=35$, $P=0.13$) with Sidak's multiple-comparisons test. **e**, Western blot of day 30 mDA cultures treated with PEP005 from multiple YOPD and control lines. **f**, Quantification of α -synuclein band intensity with and without PEP005 across multiple differentiations (CTR: $n=8$, $P<0.0001$; PD: $n=10$, $P<0.0001$) relative to untreated cells of the same line. **g,h**, Band intensity of p-PKC α (CTR: $n=4$, $P<0.0001$; PD: $n=6$, $P<0.0001$) (**g**) and LAMP1 (CTR: $n=5$, $P=0.2$; PD: $n=9$, $P=0.03$) (**h**) in cells with and without PEP005 relative to untreated cells of the same line. In **f-h**, an asterisk indicates significance relative to untreated cells determined by two-tailed paired t -test. **i**, Baseline levels of total PKC α and p-PKC α in day 30 mDA cultures. **j**, Quantification of total PKC α band intensity relative to control cells (CTR, $n=3$; PD, $n=3$). **k**, Quantification of p-PKC α band intensity relative to control cells (CTR, $n=6$; PD, $n=6$). Each point represents a separate differentiation and western blot. * $P=0.01$ relative to control cells by two-tailed t -test with Welch's correction. Bar graphs show the mean \pm s.d.

samples showed that SNCA expression was downregulated 4 h after PEP005 treatment (Extended Data Fig. 8f) and TH expression was upregulated at roughly 8 h (Extended Data Fig. 8g), suggesting an antagonistic link between the two proteins³⁹.

Confirmation of YOPD phenotypes in additional patients. We next confirmed these findings in a wider range of YOPD and control samples by deriving an additional nine YOPD and seven control lines (Supplementary Table 1) from the Lothian Birth Cohort, a group of individuals who reached 83 years of age with no signs of neurodegeneration or cognitive decline⁴⁰. All new iPSC lines differentiated similarly into mDA cultures (Extended Data Fig. 9a). To determine the reproducibility of α -synuclein accumulation across clones of the same line, three independent clonal lines were derived from the ED044iCTR and 192iPD samples differentiated as before in triplicate and TH and α -synuclein protein levels were then examined by western blot (Extended Data Fig. 9b). Quantification showed that all three clones from the ED044iCTR and 192iPD lines

produced similar TH and α -synuclein levels by line (Extended Data Fig. 9c). Consistent with previous data, 192iPD clones contained significantly more α -synuclein than controls.

A single clone from all lines in our new larger cohort was differentiated for 30 d in at least three independent experiments and probed for α -synuclein accumulation and increased p-PKC α . We integrated all data from the new lines across multiple independent differentiations with data from control and YOPD lines in our original cohort to present a full dataset from 10 control individuals and 12 patients with YOPD. To present this large dataset, z scores generated from relative α -synuclein levels were compared across all western blots with up to eight replicate differentiations per line (Fig. 5a). A patient line was considered positive if one differentiation returned a normalized α -synuclein level >1 s.d. above the median relative α -synuclein level for the entire set. We positively identified nine patients with YOPD and all ten control individuals. Patient lines were considered borderline if at least one differentiation run returned a normalized α -synuclein level >0.75

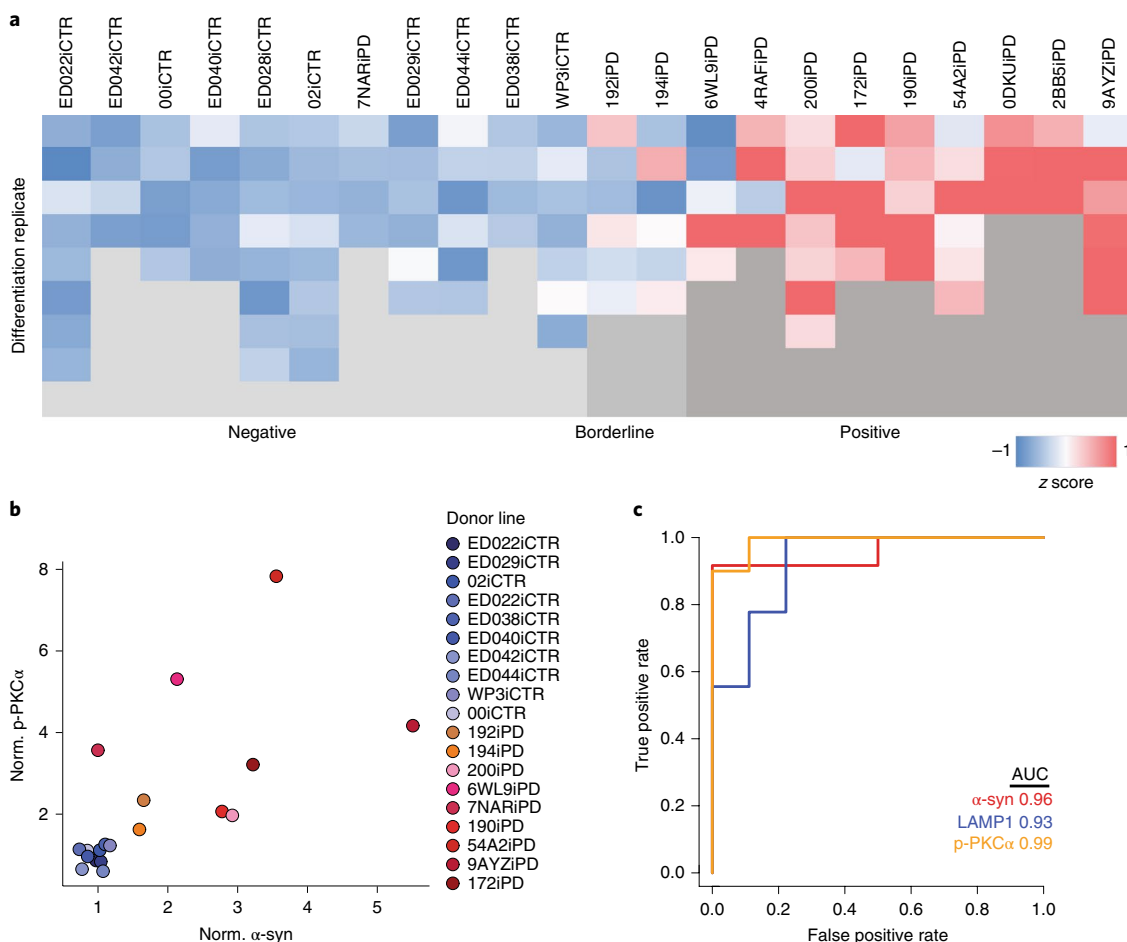


Fig. 5 | YOPD signatures across 10 control individuals and 12 patients with YOPD. a, Heat map summarizing α -synuclein expression data from all 10 control individuals and 12 patients with YOPD across multiple rounds of differentiation (each independent differentiation is a separate row). The color scale corresponds to z scores calculated from expression values detected by western blot. All values were normalized first to loading control (β -actin) and then to the average for all control lines run on the same gel. Patient lines were considered positive if at least one differentiation returned a normalized α -synuclein level >1 s.d. above the median relative α -synuclein level for the entire set. Patient lines were considered borderline if at least one differentiation run returned a normalized α -synuclein level >0.75 s.d. above the median relative α -synuclein level for the entire set (192iPD and 194iPD). **b**, Scatterplot based on normalized α -synuclein and p-PKC α levels. All values were normalized first to loading control (β -actin) and then to the average signal for all control lines run on the same gel. **c**, ROC curve plot of normalized expression averaged by cell line: α -synuclein (red), $n=22$ lines; LAMP1 (blue), $n=6$ lines; p-PKC α (orange), $n=19$ lines. Norm., normalized.

s.d. above the median relative α -synuclein level for the entire set (192iPD and 194iPD). Confirming our earlier findings, controls did not accumulate α -synuclein or display increased p-PKC α , whereas eight of the nine new patients with YOPD had both markers (Fig. 5b). Interestingly, mDA cultures from one of the new YOPD lines (7NARiPD) only displayed elevated p-PKC α levels but not altered α -synuclein. To assess the potential of α -synuclein and p-PKC α expression detection as a predictive tool for YOPD, we plotted the normalized expression values on a receiver operating characteristic (ROC) curve (Fig. 5c). The predictive accuracy of distinguishing YOPD from controls, reflected in the area under the curve, was 0.96 for α -synuclein (red), 0.93 for LAMP1 (blue) and 0.99 for p-PKC α (orange), indicating that these phenotypic markers could accurately segregate the patients in our cohort.

Additional phorbol esters alter α -synuclein and TH levels in mDA cultures. To further probe the mechanism of interaction between PEP005 and α -synuclein, we tested two additional PKC agonists with similar chemical structures to PEP005: phorbol 12-myristate 13-acetate (PMA) and prostratin (PRO) (Fig. 6a and

Extended Data Fig. 10a). Both phorbol ester compounds exhibited similar activity to PEP005, with treatment of mDA culture causing p-PKC α and α -synuclein reduction and a corresponding increase in TH (Fig. 6a).

PEP005 modulates α -synuclein independently of p-PKC α . We next conducted dose–response studies with PEP005 and PRO treatment of mDA cultures (Fig. 6b and Extended Data Fig. 10b,c). PEP005 produced a clear dose–response relationship for the drug’s direct target, p-PKC α . Interestingly, low PEP005 doses that did not alter p-PKC α levels still caused a robust reduction in α -synuclein (Fig. 6b), suggesting that the mode of action for PEP005 in reducing α -synuclein may be independent from p-PKC α . PRO decreased p-PKC α and α -synuclein levels in a dose-dependent manner, but was not as efficient as PEP005 in decreasing α -synuclein levels, suggesting a lower-affinity interaction with α -synuclein-modulating pathways.

Given the differential response of α -synuclein and p-PKC α to PEP005 at low doses and the fact that additional drugs had a similar effect to PEP005 treatment, we performed *in silico* modeling

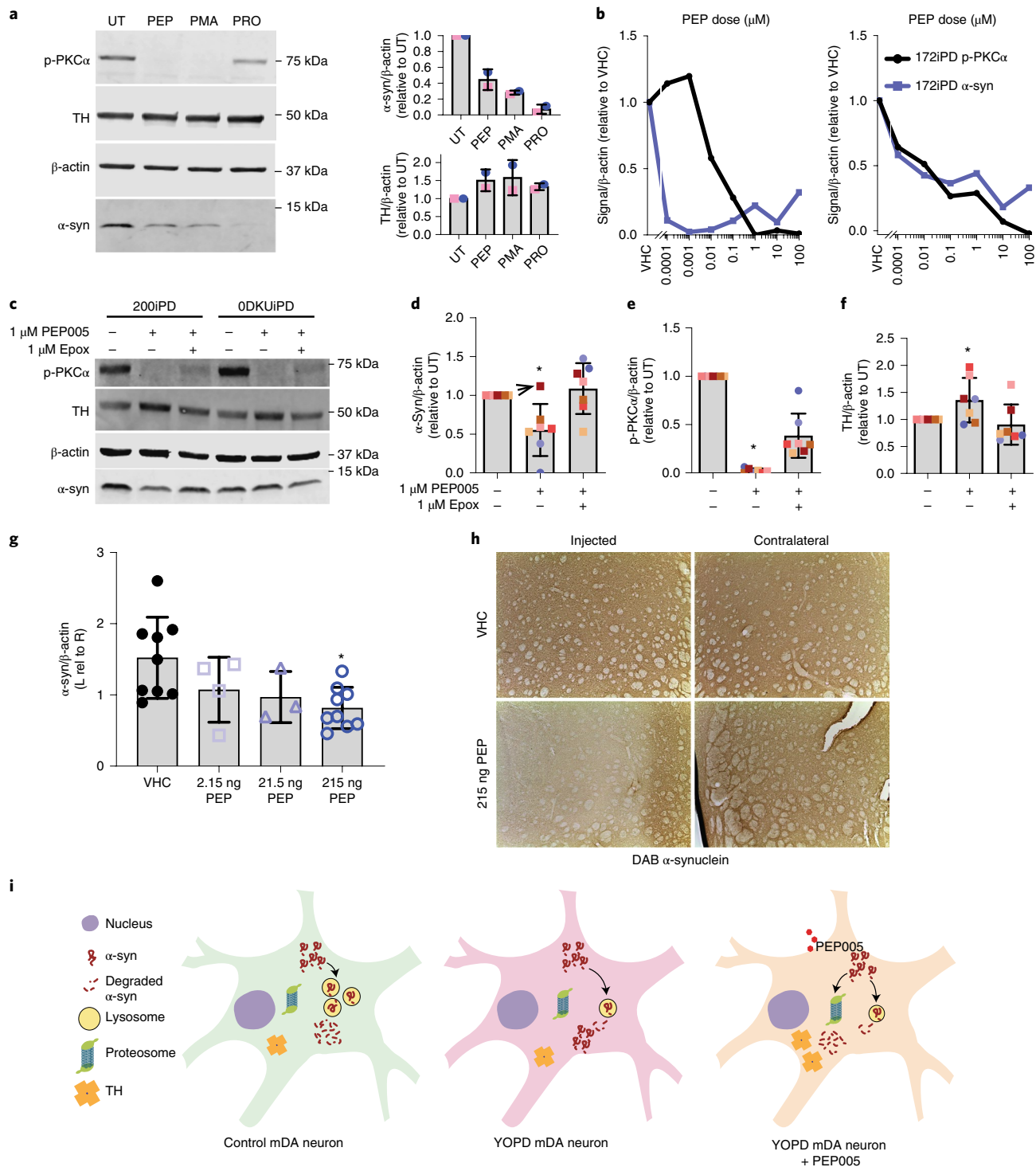


Fig. 6 | Confirmation of the effects and mechanism of PEP005. a, Treatment of mDA cultures with additional phorbol esters and quantification of band intensity from a single experiment. **b**, PEP005 and PRO dose-response curves in 172iPD mDA culture. **c–f** Western blot of d30 mDA cultures treated with the indicated compounds for 24 h (**c**) and relative quantification of α -synuclein ($n=7$; $F=7.8$, $d.f.=20$, $P=0.017$; the arrow indicates the ODKUiPD non-responder line) (**d**), p-PKC α ($n=7$; $F=96.6$, $d.f.=20$, $P<0.0001$) (**e**) and TH ($n=7$; $F=3.9$, $d.f.=20$, $P=0.04$) (**f**) levels by iPSC line. **g**, Western blot quantification of α -synuclein in mouse striatum presented as injected (left) over contralateral (right) side in response to PEP005 dose. $n=9$ mice with vehicle (VHC), $n=4$ mice with 2.15 ng PEP005, $n=3$ mice with 21.5 ng PEP005 and $n=9$ mice with 215 ng PEP005. $*P=0.015$ by one-way ANOVA ($F=3.96$, $d.f.=24$) with Tukey multiple-comparisons test. **h**, Immunohistochemical staining of α -synuclein in mouse striatum treated with 215 ng PEP005 for 3 d. **i**, Schematic representation of YOPD biomarkers and proposed mechanism of activity for PEP005. In control and YOPD mDA neurons, α -synuclein is degraded primarily via lysosomal means. However, as YOPD mDA cultures have lower abundance of lysosomal proteins, this degradation process is less efficient and results in accumulation of α -synuclein. When these cells are treated with PEP005, an alternative proteasomal mode of α -synuclein degradation is triggered in addition to the endogenous lysosomal degradation machinery, resulting in a rapid decrease in α -synuclein protein levels and a subsequent increase in TH levels. Bar graphs show the mean \pm s.d.

of potential PEP005 binding sites to identify new drug-binding partners. As expected, we confirmed several target sites with similar affinity for PEP005 binding on PKC α , but interestingly we also found binding sites on multiple additional proteins (Extended Data Fig. 10d). This suggested that PEP005 binds the GTPase RAS with similar affinity to PKC α (Extended Data Fig. 10e). RAS has a direct impact on cell proliferation through the MAPK pathway and on lysosomal biogenesis through the mTORC pathway^{41,42}.

PEP005 activates proteasomal degradation of α -synuclein. Because α -synuclein protein was substantially degraded by PEP005 without altering lysosomal proteins over the first 24 h of treatment, we investigated activation of proteasomal degradation as a potential mechanism for α -synuclein reduction. We treated day 29 mDA cultures with vehicle, 1 μ M PEP005 or 1 μ M PEP005 + 1 μ M epoxomicin. Interestingly, epoxomicin blocked PEP005-mediated reduction in α -synuclein and p-PKC α levels (Fig. 6c–e) and prevented increased TH expression (Fig. 6f). On the basis of these additional mechanistic studies, we consider that PEP005's mode of action may be related to stimulation of proteasomal degradation of α -synuclein, a pathway specifically not active in untreated neurons, rather than stimulation of lysosomal function and autophagy. The lack of altered LC3 I and LC3 II ratios (Extended Data Fig. 8b,c) supports the fact that PEP005 does not activate autophagic function. Further, the significant increase in lysosomal proteins in YOPD cultures (Fig. 4h) only occurred 72 h after PEP005 treatment, whereas α -synuclein levels were substantially reduced by 8 h (Extended Data Fig. 8d,e), suggesting that the increase in lysosomal proteins happened after α -synuclein levels had already been reduced through proteasomal means.

PEP005 reduces α -synuclein levels in vivo. Finally, to assess whether PEP005 could also reduce α -synuclein levels in vivo, mice received unilateral striatal injections of PEP005 (2.15 ng, 21.5 ng and 215 ng). Western blot and immunohistochemical assessment of the striatum at 3 d after treatment showed that the 215 ng dose significantly reduced α -synuclein levels relative to the contralateral side (Fig. 6g,h), demonstrating that PEP005 also reduces α -synuclein levels in vivo.

Discussion

PD is proposed to be caused by genetic or environmental factors or some combination thereof and in nearly all cases involves abnormal accumulation of α -synuclein. We focused on patients with young-onset disease (approximately 10% of the PD population)²¹ and have now identified a reliable molecular signature in iPSC-derived mDA cultures that correctly predicted 21 of 22 patients in this study as having PD. As iPSC generation clears most epigenetic memory⁸, this molecular signature indicates a genetic contribution to YOPD, presumably involving unknown pathogenic and modifying genes, perhaps related to some of the PD risk alleles identified in these patients (Supplementary Table 2a). Consistent with previous studies of adult-onset sporadic PD^{10,15}, a patient with adult-onset disease in the current study did not accumulate α -synuclein or have increased p-PKC α (data not shown). The failure of adult-onset PD cells to reproduce YOPD phenotypes indicates that more time in culture may be necessary to manifest these phenotypes or that the accelerated nature of YOPD represents a distinct subpopulation of PD with a deficiency in handling α -synuclein that can be readily reproduced in vitro. As with our work overexpressing α -synuclein in embryonic stem cell-derived dopamine neurons⁴³, the acute increase in soluble α -synuclein did not cause dopamine neuron death in iPSC-derived mDA cultures from patients. We hypothesize that an inability to degrade α -synuclein over many years leads to accumulation of insoluble α -synuclein in dopaminergic neurons, cellular death and Lewy body formation.

Genome-wide association studies on large cohorts of patients with sporadic disease have identified allelic variants relating to protein degradation, implicating lysosomal degradation pathways in disease pathogenesis⁴⁴. Our results support the findings of studies that indicate lysosome dysfunction as a major contributor to PD^{45,46}. While the patients with YOPD did not carry known lysosomal risk variants or display altered lysosomal gene transcription at the pathway level, lysosomal proteins and hydrolase activity were significantly reduced, suggesting that altered lysosomal protein biogenesis and stability may contribute to YOPD-specific accumulation of α -synuclein. Mitochondrial dysfunction and impaired mitophagy have been reported in patient iPSC-derived PARK2 dopamine neurons^{47–49}, and mitochondrial dysfunction occurs in iPSC models of neurodegenerative diseases including Alzheimer's disease⁵⁰ and ALS⁵¹. While mitochondria-related terms were upregulated across the whole YOPD cohort, these lost significance when the 190iPD line was removed from paired-omics analysis, indicating that the mitochondrial phenotype was largely driven by this single line.

Through activation of a previously unutilized proteasomal degradation mechanism, we were able to effect a decrease in α -synuclein protein levels. Additionally, treatment with phorbol ester compounds not only reduced α -synuclein levels but also increased the TH amount present in mDA cultures of control and PD origin. Studies have suggested an antagonistic link between α -synuclein and TH expression^{39,52}; however, as increased TH levels were specific to PEP005 treatment, the interaction may be more complex than a simple direct link. Control mDA cultures treated with SMER28 and YOPD cultures treated with trehalose showed reduced α -synuclein levels but, unlike with the phorbol esters, neither reduction produced an increase in the amount of TH enzyme. These divergent results suggest that the two pathways may converge on a common target but are otherwise independent (Fig. 6i). Because α -synuclein, TH and TFEB all bind to the 14-3-3 scaffold proteins^{53–55} and PEP005 treatment alters all three pathways, we hypothesize that the 14-3-3 proteins act as a central hub for this interaction.

The dual effects of reducing intracellular α -synuclein and increasing TH levels make PEP005 a very attractive candidate for a potential therapeutic agent. PEP005 is a US Food and Drug Administration (FDA)-approved drug for topical treatment of actinic keratosis that also has antileukemic activity and may play a role in reactivating latent HIV^{56,57}. It was selected here as a structural analog derived from the same plant as the HEP14 compound that acts as a TFEB agonist, independently of the mTORC pathway³⁶. Treated control and YOPD cells showed an increase in the lysosomal protein LAMP1 consistent with activation of the lysosomal master regulator TFEB. Network analysis of proteomic data also suggested TFEB to be central to downregulation of lysosomal pathways in YOPD mDA cultures. Even though we initially approached PEP005 as a potential lysosomal and TFEB agonist, the time course of effects suggested an alternative mode of action. We observed reduced α -synuclein levels within 8 h of PEP005 addition; however, lysosomal proteins were not altered at this time point nor was there any stimulation of bulk autophagy. Furthermore, addition of the specific proteasomal inhibitor epoxomicin blocked PEP005-induced α -synuclein degradation, indicating activation of proteasomal degradation of α -synuclein as the main mode of action.

Investigating the mechanism of action of PEP005 revealed increased levels of p-PKC α that were specific to the YOPD mDA cultures. While associated with certain cancers³⁸, this is a new signal in the PD literature. Our p-PKC α findings in iPSC-derived mDA cultures provide an exciting molecular marker for PD, which we plan to further validate in postmortem PD tissue. Three of our tested PKC agonists (phorbol esters) all decreased p-PKC α , which was accompanied by reduced α -synuclein and increased TH levels. Additionally, the dose–response studies indicated that PEP005 can alter α -synuclein levels without substantially affecting p-PKC α .

These results would suggest that some interaction specific to the structure of the phorbol ester compounds is driving the decreased α -synuclein and not the reduction of p-PKC α . Interestingly, PKC and protein kinase A (PKA), which are more heavily phosphorylated in YOPD cells, are negative upstream regulators of sodium ion channels³⁹. This may explain the observed decrease in sodium current amplitude from patched YOPD mDA cultures.

The inherent patient specificity of this model presents the opportunity for development of YOPD diagnostics and therapeutics that can be used before symptom onset. Every control line had low α -synuclein levels and so there was no case of a 'false positive'. One clinically confirmed patient with YOPD (7NARIPD) did not exhibit the increase in α -synuclein levels and hence was not correctly identified. This suggests that, although the model was 96% sensitive and robust in its predictive power across 23 patients, not all patients with YOPD can be identified by elevated α -synuclein. This type of phenotypic discrepancy may indicate a diverse etiology of PD and therefore could provide valuable preclinical data, such as inclusion criteria for mechanistic studies and clinical trials. Indeed, one patient (0DKUiPD) did not respond to PEP005 treatment. This nonresponse may be driven by a unique genetic deficiency and further highlights the utility of this assay as a screen for clinical trial inclusion. Studies in synucleinopathy animal models, such as the THY-1 synuclein mouse⁶⁰, would provide further insight into the efficacy of PEP005 and other phorbol esters as therapeutic candidates. Such studies could also be used to determine an efficient route of delivery for PEP005, which has been approved by the US FDA as a topical agent.

This work identifies a molecular signature in an iPSC-based model of YOPD, thereby demonstrating an unexpected and clear genetic contribution to a PD population previously considered as sporadic. The combination of accumulation of α -synuclein, dysregulation of lysosomal biogenesis and function, and increases in p-PKC α was a highly predictive phenotype in our model of YOPD, and thus represents a new diagnostic tool for clinicians. This may be particularly valuable for at-risk individuals from families with one proband with YOPD. Finally, our work could provide a screening platform for new therapeutic agents that impact the underlying mechanisms in YOPD. For example, we have identified drugs that target this signature and reduce intracellular α -synuclein levels in control and disease-derived cells. These phorbol ester drugs, in particular PEP005, may treat the underlying cause of YOPD and could uncover shared principles with other neurodegenerative disorders. A definitive diagnosis could initiate phorbol ester-based drug treatment early in disease to reduce α -synuclein accumulation and increase TH levels, both of which could have potentially stabilizing effects to delay disease onset and slow progression.

Online content

Any methods, additional references, Nature Research reporting summaries, source data, extended data, supplementary information, acknowledgements, peer review information; details of author contributions and competing interests; and statements of data and code availability are available at <https://doi.org/10.1038/s41591-019-0739-1>.

Received: 15 October 2018; Accepted: 16 December 2019;

Published online: 27 January 2020

References

- Puschmann, A. Monogenic Parkinson's disease and Parkinsonism: clinical phenotypes and frequencies of known mutations. *Parkinsonism Relat. Disord.* **19**, 407–415 (2013).
- Kalia, L. V. & Lang, A. E. Parkinson's disease. *Lancet* **386**, 896–912 (2015).
- Spillantini, M. G. et al. α -Synuclein in Lewy bodies. *Nature* **388**, 839–840 (1997).
- Lashuel, H. A., Overk, C. R., Oueslati, A. & Masliah, E. The many faces of α -synuclein: from structure and toxicity to therapeutic target. *Nat. Rev. Neurosci.* **14**, 38–48 (2013).
- Singleton, A. B. et al. α -Synuclein locus triplication causes Parkinson's disease. *Science* **302**, 841–841 (2003).
- Shi, Y., Inoue, H., Wu, J. C. & Yamanaka, S. Induced pluripotent stem cell technology: a decade of progress. *Nat. Rev. Drug Discovery* **16**, 115–130 (2017).
- Studer, L., Vera, E. & Cornacchia, D. Programming and reprogramming cellular age in the era of induced pluripotency. *Cell Stem Cell* **16**, 591–600 (2015).
- Kim, K. et al. Epigenetic memory in induced pluripotent stem cells. *Nature* **467**, 285–290 (2010).
- Woodard, Chris M. et al. iPSC-derived dopamine neurons reveal differences between monozygotic twins discordant for Parkinson's disease. *Cell Rep.* **9**, 1173–1182 (2014).
- Soldner, F. et al. Parkinson's disease patient-derived induced pluripotent stem cells free of viral reprogramming factors. *Cell* **136**, 964–977 (2009).
- Byers, B. et al. SNCA triplication Parkinson's patient's iPSC-derived DA neurons accumulate α -synuclein and are susceptible to oxidative stress. *PLoS One* **6**, e26159 (2011).
- Devine, M. J. et al. Parkinson's disease induced pluripotent stem cells with triplication of the α -synuclein locus. *Nat. Commun.* **2**, 440 (2011).
- Oliveira, L. M. et al. Elevated α -synuclein caused by SNCA gene triplication impairs neuronal differentiation and maturation in Parkinson's patient-derived induced pluripotent stem cells. *Cell Death Dis.* **6**, e1994 (2015).
- Schondorf, D. C. et al. iPSC-derived neurons from GBA1-associated Parkinson's disease patients show autophagic defects and impaired calcium homeostasis. *Nat. Commun.* **5**, 4028 (2014).
- Sanchez-Danes, A. et al. Disease-specific phenotypes in dopamine neurons from human iPSC-based models of genetic and sporadic Parkinson's disease. *EMBO Mol. Med.* **4**, 380–395 (2012).
- Sanders, L. H. et al. LRRK2 mutations cause mitochondrial DNA damage in iPSC-derived neural cells from Parkinson's disease patients: reversal by gene correction. *Neurobiol. Dis.* **62**, 381–386 (2014).
- Schwab, A. J. & Ebert, A. D. Neurite aggregation and calcium dysfunction in iPSC-derived sensory neurons with Parkinson's disease-related LRRK2 G2019S mutation. *Stem Cell Rep.* **5**, 1039–1052 (2015).
- Schrag, A. & Schott, J. M. Epidemiological, clinical, and genetic characteristics of early-onset Parkinsonism. *Lancet Neurol.* **5**, 355–363 (2006).
- Rizek, P., Kumar, N. & Jog, M. S. An update on the diagnosis and treatment of Parkinson disease. *CMAJ* **188**, 1157–1165 (2016).
- Pagano, G., Ferrara, N., Brooks, D. J. & Pavese, N. Age at onset and Parkinson disease phenotype. *Neurology* **86**, 1400–1407 (2016).
- Alcalay, R. N. et al. Frequency of known mutations in early-onset parkinson disease: implication for genetic counseling: the consortium on risk for early-onset Parkinson disease study. *Arch. Neurol.* **67**, 1116–1122 (2010).
- Ebert, A. D. et al. Induced pluripotent stem cells from a spinal muscular atrophy patient. *Nature* **457**, 277–280 (2009).
- Nalls, M. A. et al. NeuroX, a fast and efficient genotyping platform for investigation of neurodegenerative diseases. *Neurobiol. Aging* **36**, 1605 e1607–1605 e1612 (2015).
- Nalls, M. A. et al. Identification of novel risk loci, causal insights, and heritable risk for Parkinson's disease: a meta-analysis of genome-wide association studies. *Lancet Neurol.* **18**, 1091–1102 (2019).
- Kriks, S. et al. Dopamine neurons derived from human ES cells efficiently engraft in animal models of Parkinson's disease. *Nature* **480**, 547–551 (2011).
- Kikuchi, T. et al. Human iPSC cell-derived dopaminergic neurons function in a primate Parkinson's disease model. *Nature* **548**, 592–596 (2017).
- Reyes, S. et al. GIRK2 expression in dopamine neurons of the substantia nigra and ventral tegmental area. *J. Comp. Neurol.* **520**, 2591–2607 (2012).
- Bennett, M. C. et al. Degradation of α -synuclein by proteasome. *J. Biol. Chem.* **274**, 33855–33858 (1999).
- Webb, J. L., Ravikumar, B., Atkins, J., Skepper, J. N. & Rubinsztein, D. C. α -Synuclein is degraded by both autophagy and the proteasome. *J. Biol. Chem.* **278**, 25009–25013 (2003).
- Mak, S. K., McCormack, A. L., Manning-Bog, A. B., Cuervo, A. M. & Di Monte, D. A. Lysosomal degradation of α -synuclein in vivo. *J. Biol. Chem.* **285**, 13621–13629 (2010).
- Xilouri, M., Brekk, O. R. & Stefanis, L. α -Synuclein and protein degradation systems: a reciprocal relationship. *Mol. Neurobiol.* **47**, 537–551 (2013).
- Mazzulli, J. R., Zunke, F., Isacson, O., Studer, L. & Krainc, D. α -Synuclein-induced lysosomal dysfunction occurs through disruptions in protein trafficking in human midbrain synucleinopathy models. *Proc. Natl. Acad. Sci. USA* **113**, 1931–1936 (2016).
- Murphy, K. E. et al. Reduced glucocerebrosidase is associated with increased α -synuclein in sporadic Parkinson's disease. *Brain* **137**, 834–848 (2014).
- Burbulla, L. F. et al. Dopamine oxidation mediates mitochondrial and lysosomal dysfunction in Parkinson's disease. *Science* **357**, 1255–1261 (2017).

35. Decressac, M. et al. TFEB-mediated autophagy rescues midbrain dopamine neurons from α -synuclein toxicity. *Proc. Natl Acad. Sci. USA* **110**, E1817–E1826 (2013).
36. Li, Y. et al. Protein kinase C controls lysosome biogenesis independently of mTORC1. *Nat. Cell Biol.* **18**, 1065–1077 (2016).
37. Sarkar, S. et al. Small molecules enhance autophagy and reduce toxicity in Huntington's disease models. *Nat. Chem. Biol.* **3**, 331–338 (2007).
38. Sarkar, S., Davies, J. E., Huang, Z., Tunnacliffe, A. & Rubinsztein, D. C. Trehalose, a novel mTOR-independent autophagy enhancer, accelerates the clearance of mutant huntingtin and α -synuclein. *J. Biol. Chem.* **282**, 5641–5652 (2007).
39. Li, Y. H. et al. α -Synuclein functions as a negative regulator for expression of tyrosine hydroxylase. *Acta Neurol. Belg.* **111**, 130–135 (2011).
40. Deary, I. J. et al. The Lothian Birth Cohort 1936: a study to examine influences on cognitive ageing from age 11 to age 70 and beyond. *BMC Geriatr.* **7**, 28 (2007).
41. Asati, V., Mahapatra, D. K. & Bharti, S. K. PI3K/Akt/mTOR and Ras/Raf/MEK/ERK signaling pathways inhibitors as anticancer agents: structural and pharmacological perspectives. *Eur. J. Med. Chem.* **109**, 314–341 (2016).
42. Rocznik-Ferguson, A. et al. The transcription factor TFEB links mTORC1 signaling to transcriptional control of lysosome homeostasis. *Sci. Signal.* **5**, ra42 (2012).
43. Schneider, B. L. et al. Over-expression of α -synuclein in human neural progenitors leads to specific changes in fate and differentiation. *Hum. Mol. Genet.* **16**, 651–666 (2007).
44. Chang, D. et al. A meta-analysis of genome-wide association studies identifies 17 new Parkinson's disease risk loci. *Nat. Genet.* **49**, 1511–1516 (2017).
45. Wong, Y. C. & Krainc, D. α -Synuclein toxicity in neurodegeneration: mechanism and therapeutic strategies. *Nat. Med.* **23**, 1–13 (2017).
46. Dehay, B. et al. Lysosomal impairment in Parkinson's disease. *Mov. Disord.* **28**, 725–732 (2013).
47. Imaizumi, Y. et al. Mitochondrial dysfunction associated with increased oxidative stress and α -synuclein accumulation in PARK2 iPSC-derived neurons and postmortem brain tissue. *Mol. Brain* **5**, 35 (2012).
48. Suzuki, S. et al. Efficient induction of dopaminergic neuron differentiation from induced pluripotent stem cells reveals impaired mitophagy in PARK2 neurons. *Biochem. Biophys. Res. Commun.* **483**, 88–93 (2017).
49. Ishikawa, K. I., Yamaguchi, A., Okano, H. & Akamatsu, W. Assessment of mitophagy in iPSC cell-derived neurons. *Methods Mol. Biol.* **1759**, 59–67 (2018).
50. Ridge, P. G. & Kauwe, J. S. K. Mitochondria and Alzheimer's disease: the role of mitochondrial genetic variation. *Curr. Genet. Med. Rep.* **6**, 1–10 (2018).
51. Fujimori, K. et al. Modeling sporadic ALS in iPSC-derived motor neurons identifies a potential therapeutic agent. *Nat. Med.* **24**, 1579–1589 (2018).
52. Yu, S. et al. Inhibition of tyrosine hydroxylase expression in α -synuclein-transfected dopaminergic neuronal cells. *Neurosci. Lett.* **367**, 34–39 (2004).
53. Halskau, O. Jr. et al. Three-way interaction between 14-3-3 proteins, the N-terminal region of tyrosine hydroxylase, and negatively charged membranes. *J. Biol. Chem.* **284**, 32758–32769 (2009).
54. Ostrerova, N. et al. α -Synuclein shares physical and functional homology with 14-3-3 proteins. *J. Neurosci.* **19**, 5782–5791 (1999).
55. Xu, Y. et al. YWHA/14-3-3 proteins recognize phosphorylated TFEB by a noncanonical mode for controlling TFEB cytoplasmic localization. *Autophagy* **15**, 1017–1030 (2019).
56. Hampson, P. et al. Kinetics of ERK1/2 activation determine sensitivity of acute myeloid leukaemia cells to the induction of apoptosis by the novel small molecule ingenol-3-angelate (PEP005). *Apoptosis* **15**, 946–955 (2010).
57. Jiang, G. et al. Synergistic reactivation of latent HIV expression by ingenol-3-angelate, PEP005, targeted NF- κ B signaling in combination with JQ1-induced p-TEFb activation. *PLoS Pathog.* **11**, e1005066 (2015).
58. Garg, R. et al. Protein kinase C and cancer: what we know and what we do not. *Oncogene* **33**, 5225–5237 (2014).
59. Scheuer, T. Regulation of sodium channel activity by phosphorylation. *Semin. Cell Dev. Biol.* **22**, 160–165 (2011).
60. Chesselet, M. F. et al. A progressive mouse model of Parkinson's disease: the Thy1-aSyn ("Line 61") mice. *Neurotherapeutics* **9**, 297–314 (2012).

Publisher's note Springer Nature remains neutral with regard to jurisdictional claims in published maps and institutional affiliations.

© The Author(s), under exclusive licence to Springer Nature America, Inc. 2020

Methods

Details on the materials and software used in this study can be found in the Nature Research Reporting Summary.

Ethics statement. All cell lines and protocols in the present study were used in accordance with guidelines approved by the Stem Cell Research Oversight committee and institutional review board under the auspice institutional review board and Stem Cell Research Oversight protocols Pro00032834 (iPSC Core Repository and Stem Cell Program) and Pro00021505 (Svendsen Stem Cell Program). All mouse work in this study was performed under the guidelines of the Cedars-Sinai Medical Center Institutional Animal Care and Use Committee under protocol 6462.

iPSC line generation. iPSC lines were generated by nucleofecting parent cells with nonintegrating oriP/EBNA1 plasmids, which allowed for episomal expression of reprogramming factors as described previously⁶¹, in collaboration with the Cedars-Sinai iPSC Core.

iPSC maintenance, mDA neuron differentiation and drug treatments. iPSCs were maintained in E8 medium on Matrigel and passaged every 5 d at split ratios from 1:6 to 1:12 as needed using Versene. Only iPSCs between passage 17 and passage 35 were used in this study. For differentiation, iPSCs were grown to ~80% confluency. Cells were singularized with Accutase (Millipore/Sigma, SCR005; 5 min at 37°C) and plated onto Matrigel-coated six-well plates (BD Biosciences) at 200,000 cells per cm² (for a fully confluent monolayer) in E8 medium with 5 μM Y27632 (StemGent). At 24 h after plating, the medium was changed to stage 1 medium (50% DMEM/F12 and 50% neurobasal, N2, B27-vitamin A, LDN-193189 (LDN) and SB431542 (SB)). Stage 1 medium was changed each day (3 ml per well) for 3 d. Medium was next switched to stage 2 medium (50% DMEM/F12 and 50% neurobasal, N2, B27-vitamin A, LDN, SB, purlmorphamine (PMN), CHIR99021 (CHIR), Sonic hedgehog (SHH) and fibroblast growth factor 8 (FGF8)). Stage 2 medium was changed each day (3 ml per well) for 4 d. Medium was then switched to stage 3 medium (50% DMEM/F12 and 50% neurobasal, N2, B27-vitamin A, LDN, CHIR and all-*trans* retinoic acid (ATRA)). Stage 3 medium was changed each day (3 ml per well) for 4 d. Finally, medium was switched to stage 4 medium (50% DMEM/F12 and 50% neurobasal, N2, B27-vitamin A, brain-derived neurotrophic factor (BDNF), glial cell line-derived neurotrophic factor (GDNF), dibutylcyclic AMP sodium salt (dbcAMP), L-ascorbic acid (AA), γ -secretase inhibitor (DAPT), CHIR and transforming growth factor- β 3). Stage 4 medium was changed each day (3 ml per well) for 3 d. On day 15, cells were dissociated to single cells using Accutase (20 min at 37°C) and gently lifted. Dissociated cells were resuspended in maturation medium (50% DMEM/F12 and 50% neurobasal, N2, B27-vitamin A, BDNF, GDNF, dbcAMP, AA, DAPT and transforming growth factor- β 3) plus 5 μM Y27632 and reseeded onto Matrigel-coated six-well plates at 200,000 cells per cm² in 1-ml total volume or onto Matrigel-coated L-glass coverslips in a 24-well plate at 200,000 cells in a 50-μl drop. Cells were allowed to attach for 45 min at 37°C and maturation medium was then added to a final volume of 3 ml per well for six-well plates or 1.5 ml per well for 24-well plates with coverslips. A full medium change was performed 48 h after seeding and medium was changed every 3 d until day 30. For drug treatments, cells at day 27 were fed with maturation medium containing the indicated drug and cells were analyzed at day 30. The drugs were as follows: 1 μM PEP005 (Tocris, 4054), 5 μM SMER28 (Tocris, 4297), 25 M trehalose (Sigma-Aldrich, T0167), 10 μM PMA (Tocris, 1201) and 5 μM PRO (Tocris, 5739). Reagents and dilutions for mDA differentiation are listed in Supplementary Table 4.

Flow cytometry quantification. Day 30 cultures in six-well plates were washed once in phosphate-buffered saline (PBS) followed by addition of 1 ml of Accutase to each well and incubation for 25 min at 37°C or until the cells fully lifted. Cells were washed with an additional 2 ml of maturation medium and very gently triturated until large clumps were no longer visible, at which point cells were pelleted by centrifugation (1,500 r.p.m. for 3 min). Cells were gently resuspended in 4% paraformaldehyde (PFA) in PBS and allowed to fix for 10–15 min at room temperature. Fixed single cells were permeabilized using 1% Triton X-100 (Sigma-Aldrich) and stained using primary antibodies against TH (1:500 dilution, Immunostar, 22941), α -synuclein (1:1,000 dilution, Abcam, ab138501) and MAP2ab (1:1,000 dilution, Sigma-Aldrich, M1406) or isotype controls at the same dilution (rabbit (3900) and mouse (5415S) IgG isotype control, Cell Signaling). Secondary antibodies (Alexa Fluor 488 and 594 donkey anti-mouse and donkey anti-rabbit, Invitrogen) were used at a 1:500 dilution. Stained samples were quantified on an LSR Fortessa cytometer using BD FACSDiva software.

Dopamine detection. To detect dopamine content and release in mDA cultures, cells were plated on L-glass coverslips and grown as above, and extracts and effluents were collected. For total dopamine, cultures were washed in artificial cerebral spinal fluid (aCSF) and immediately lysed in 200 μl of 0.2 M perchloric acid and 0.1 mM EDTA. Lysates were flash frozen in liquid nitrogen. To detect released dopamine on day 30, culture medium was aspirated and cells were washed twice with aCSF. After washing, 200 μl of aCSF was carefully added on top of each

coverslip, incubated at 37°C for 15 min and collected. Then, 200 μl of high-K⁺ aCSF was added to the top of each coverslip, incubated for 15 min and collected. Immediately after collection, 20 μl of 10× stabilization buffer (2 M perchloric acid and 1 mM EDTA) was added to each sample. Stabilized samples were snap frozen in liquid nitrogen and stored at –80°C until HPLC analysis. Separation was performed on a 2.1 × 100 mm × 3 μm reversed-phase Hypersil ODS column with a mobile phase consisting of 75 mM sodium acetate, 0.75 mM SDS, 2.5% acetonitrile, 12.5% methanol and 10 μM EDTA (pH 5.5) pumped at a rate of 0.2 ml min⁻¹. Electrochemical detection of dopamine was conducted at a glassy carbon electrode held at a potential of 0.45 V versus an Ag/AgCl reference electrode and provided a limit of detection of 0.1 nM for a 10-μl injection. Samples were analyzed in triplicate against known standard concentrations of dopamine.

Immunocytochemistry and imaging. mDA neuron cultures were plated on L-glass coverslips and grown as above. Day 30 neurons were fixed in 4% PFA at room temperature for 10–15 min. Fixed coverslips were washed in PBS and permeabilized for 10 min at room temperature in 1% Triton X-100 in PBS, followed by staining in primary antibody solution (5% normal donkey serum and 0.125% Triton X-100 in PBS) overnight at 4°C with the following antibodies: TH (1:5,000 dilution, Immunostar, 22941) and α -synuclein (1:500 dilution, Abcam, ab138501). Samples were washed three times in PBS and stained with species-specific Alexa Fluor 488- or Alexa Fluor 594-conjugated secondary antibodies (1:500 dilution, Invitrogen) for 2 h at room temperature, followed by DAPI counterstain. Confocal z-stack images were acquired using an A1 microscope (Nikon) with ×40 and ×20 objectives and rendered using maximum-intensity projection through IMARIS software (Bitplane).

Western blots. Cells were gently scraped off the plates, washed with PBS and centrifuged at 15,000 r.p.m. for 1 min. Dry pellets were frozen at –80°C. Samples were then thawed and lysed using 1× NETN buffer (20 mM Tris-HCl (pH 8.0), 100 mM NaCl, 0.5 mM EDTA and 0.5% NP-40) supplemented with phosphatase-protease inhibitor cocktail (MS-SAFE, Sigma-Aldrich). Lysates were sonicated in an automated cold bath sonicator for 20 min using alternating 10-s pulses followed by 10-s rests. Samples were centrifuged for 20 min at 4°C at 15,000 r.p.m. Total soluble protein concentrations were measured using a Bradford assay (Bio-Rad). Then, 4× Laemmli sample buffer (Bio-Rad, 161-0774) was added to either 100 μg or 50 μg of total protein extracts and samples were boiled for 5 min. Samples were run in 4–20% Mini-PROTEAN TGX precast gels (Bio-Rad, 456-1094) and transferred to polyvinylidene difluoride (PVDF) membranes using the Trans-Blot Turbo Transfer System (Bio-Rad). Membranes were blocked with Odyssey blocking buffer (LI-COR) and then incubated with primary antibodies overnight at 4°C or room temperature for 3 h. Following incubation with dye-labeled secondary antibodies for 2 h at room temperature, signals were visualized using an Odyssey Fc imaging system (LI-COR). Primary antibodies used were human α -synuclein (1:1,000 dilution, Abcam, ab138501), mouse α -synuclein (1:1,000 dilution, Abcam, ab212184), TH (1:2,000 dilution, Immunostar, 22941), total PKC α (1:1,000 dilution, Cell Signaling, 2056), p-PKC α (1:1,000 dilution, Cell Signaling, 9375), LAMP1 (1:1,000 dilution, Cell Signaling, 9091), LCI/II (1:1,000 dilution, Cell Signaling, 12741), cleaved caspase 3-CC3 (1:1,000 dilution, Cell Signaling, 9661), synaptophysin (1:1,000 dilution, Abcam, ab32127), p53 (1:2,000 dilution, Santa Cruz, sc-126), glyceraldehyde 3-phosphate dehydrogenase (GAPDH; 1:5,000 dilution, Sigma-Aldrich, G8795) and β -actin (1:5,000 dilution, Sigma-Aldrich, A5441). Secondary antibodies were IRDye 680 RD goat anti-mouse and IRDye 800CW goat anti-rabbit (LI-COR, 926-68070 and 926-32211, respectively) at a dilution of 1:5,000. Combined α -synuclein and p-PKC α expression plots were calculated by first normalizing bands to β -actin and then to the 02ICTR signal present in each blot. All values were then compared across at least three independent differentiations for each line. For p-PKC α and total PKC α , the same biological lysates were run with the same volume (protein concentration) on separate blots. Because the molecular weights of p-PKC α and total PKC α were nearly identical on the gradient gels and the host species of both antibodies was the same, separate gels were required to clearly quantify both species of the protein. ROC plots and areas under the curve were determined using the R package ROCR to determine predicative probability percentages. Whole western blots for each protein are presented in Supplementary Data 1 for the western blots used in the main figures and in Supplementary Data 2 for the western blots used in Extended Data figures. In instances of partial blots, the membranes had been cut before antibody staining to use antibodies from the same species on a single western run.

CN-PAGE western blots. Cells were gently scraped off the plates, washed with PBS and lysed using 1× NETN buffer supplemented with phosphatase-protease inhibitor cocktail. Lysates were sonicated in an automated cold bath sonicator for 20 min using alternating 10-s pulses followed by 10-s rests. Samples were centrifuged for 20 min at 4°C at 15,000 r.p.m. Soluble fractions were separated into new tubes, and the remaining insoluble pellets were washed with NETN buffer to remove residual soluble protein. Total soluble protein concentrations were measured using a Bradford assay (Bio-Rad). The 1× loading buffer (40 mM Tris-HCl (pH 6.8), 4% glycerol, 0.01% bromophenolblue and 5% β -mercaptoethanol) without SDS was added to 100 μg of total soluble protein or the entire insoluble

pellet of each sample. All samples were then sonicated for 3 min with a benchtop ultrasonicator at 40% power. Samples were boiled for 10 min, run in nondenaturing Mini-PROTEAN TGX precast gels (Bio-Rad, 456–1094) with Tris-glycine running buffer (25 mM Tris-HCl and 200 mM glycine) and transferred to PVDF membranes using the Trans-Blot Turbo Transfer System (Bio-Rad). Membranes were blocked with Odyssey blocking buffer (LI-COR) and then incubated first in primary rabbit anti- α -synuclein solution overnight at 4°C. Following incubation with an anti-rabbit dye-labeled secondary antibody for 2 h at room temperature, α -synuclein signal was visualized using an Odyssey Fc imaging system (LI-COR). To establish loading controls after imaging, whole membranes were washed in TBST buffer, re-blocked with Odyssey blocking buffer for 30 min at room temperature and incubated with a primary mouse anti- β -actin antibody at room temperature for 3 h. Following incubation with an anti-mouse dye-labeled secondary antibody for 2 h at room temperature, signals were again visualized using an Odyssey Fc imaging system (LI-COR).

qPCR. Total cellular RNA was isolated using TRIzol reagent followed by a Qiagen RNeasy Mini kit with DNase treatment. Total RNA (1 μ g) was used for cDNA synthesis using the Quantitate Reverse Transcription kit for cDNA Synthesis for PCR (Qiagen). Real-time PCR was performed using SYBR Green Supermix (Bio-Rad). The levels of expression of respective genes were normalized to corresponding *GAPDH* values and are shown as fold change relative to the value of the control sample ($\Delta\Delta C_t$, method). All sample analyses were carried out in triplicate. Primers (IDT) used for real-time PCR experiments are listed in Supplementary Table 5.

NIRF detection of oxidized dopamine. Assays were performed as described by Burbulla et al.³⁴. Briefly, neurons were scrapped in cold PBS and centrifuged at 15,000 r.p.m. for 1 min. The cell pellet was frozen and then thawed and homogenized in 1 \times NETN lysis buffer with a phosphatase–protease inhibitor cocktail. Lysates were sonicated in a bath sonicator for 10 min and spun at 15,000 r.p.m. for 15 min. Supernatant was removed and the insoluble pellets were resuspended in 20 μ l of 18 M Ω distilled water. Total protein was measured using a Bradford assay and 100 μ g of protein was brought up in 20 μ l and dropped onto a Biotyne Nylon Transfer Membrane (Pall, Pall-60209). Membranes were scanned using an Odyssey infrared imaging system (LI-COR) with the 700 channel. Samples were quantified by obtaining integrated spot intensities using Odyssey infrared imaging software, v.3.1.

GCase activity with 4-methylumbelliferyl β -glucopyranoside. Assays were performed as described previously^{62,63}. Briefly, samples were lysed as above and centrifuged at 15,000 r.p.m. for 15 min at 4°C. Then, 50 μ g of total protein was incubated in activity assay buffer (0.25% (vol/vol) Triton X-100 and 1 mM EDTA, in citrate-phosphate buffer, pH 5.4) in 1% BSA, with 1 mM 4-methylumbelliferyl β -glucopyranoside (4-MU; Sigma-Aldrich, M3633) in a 200- μ l total volume. After incubation for 40 min at 37°C, the reaction was stopped by addition of an equal volume of 1 M glycine (pH 12.5). Then, 100- μ l replicates were loaded into white 96-well plates (Corning Assay plates) and fluorescence (excitation, 355 nm; emission, 460 nm) was determined in a Molecular Devices SpectraMax i3 Multi-Mode microplate reader with SoftMax Pro software.

Transcriptomics. Triplicate wells for each line were differentiated as above and split into cell pellets for either mRNA sequencing or proteomic analysis. mRNA was isolated using previously described methods⁶⁴. Briefly, library construction was performed using the Illumina TruSeq Stranded mRNA library preparation kit (Illumina). Total RNA samples were assessed for concentration using a Qubit fluorometer (Thermo Fisher) and for quality using the 2100 Bioanalyzer (Agilent Technologies). Up to 1 μ g of total RNA per sample was used for poly(A) mRNA selection. cDNA was synthesized from enriched and fragmented RNA using reverse transcriptase (Invitrogen) and random primers. cDNA was further converted into double-stranded DNA (dsDNA), and the resulting dsDNA was enriched with PCR for library preparation. The PCR-amplified library was purified using Agencourt AMPure XP beads (Beckman Coulter). The concentration of the amplified library was measured with a Qubit fluorometer and an aliquot of the library was resolved on a Bioanalyzer. Sample libraries were multiplexed and sequenced on the NextSeq 500 platform (Illumina) using 75-bp single-end sequencing. On average, about 20 million reads were generated from each sample. Raw reads obtained from RNA-seq were aligned to the transcriptome using STAR (v.2.5.0)⁶⁵ and RSEM (v.1.2.25)⁶⁶ with default parameters, using a custom human GRCh38 (or mouse CRCm38) transcriptome reference downloaded from <http://www.genecodegenes.org>, containing all protein-coding and long noncoding RNA genes based on human GENCODE v.23 (or mouse GENCODE M8) annotation. Expression counts for each gene (transcripts per million, TPM) in all samples were normalized by the sequencing depth. To determine detected transcripts, a filter of >0.1 TPM in at least nine samples was used as a threshold for detection of a unique transcript (Cluster 3.0). PCA was conducted on log-transformed data using Cluster 3.0 software.

Proteomics. Frozen pellets were lysed using 2% SDS + 10 mM TCEP (Tris 2-carboxyethyl phosphine) buffer and sonicated. The BCA assay (Pierce, 23225)

was used to determine protein concentration and 125 μ g of protein was digested using FASP Protein Digestion kits (Expedeon). A total of 3.125 μ g of trypsin-LysC was used to digest each sample overnight at 37°C with shaking at 1,000 r.p.m. Samples were desalted using an Oasis MCX μ elution plate and were eluted with 300 μ l of methanol/ammonium hydroxide. Samples were dried in a SpeedVac and resuspended in Biognosys iRT solution. Sample/iRT solution (4 μ g) was loaded onto an Eksigent 415 LC connected to a 6600 TripleTOF (Sciex) operating in microflow mode. Peptides were preloaded onto the trap column (ChromXP, C18CL; 10 \times 0.3 mm \times 5 μ m, 120 Å) at a flow rate of 10 μ l min⁻¹ for 3 min and separated on the analytical column with a temperature of 30°C (ChromXP, C18CL; 150 \times 0.3 mm \times 3 μ m, 120 Å) and a flow rate of 5 μ l min⁻¹. For DIA samples, the peptides were separated using a linear A–B gradient composed of 3–30% A for 38 min, 30–40% B for 5 min, 40–85% B for 2 min, an isocratic hold at 85% for 3 min and re-equilibration at 3% A for 8 min. Data were acquired for 400–1,250 *m/z* with an MS1 scan of 150 ms and 100 variable-window MS2 scans of 25 ms. Source parameters were set to the following values: gas 1 = 15, gas 2 = 20, curtain gas = 25, source temp = 100 and voltage = 5,500 V. Data-dependent-acquisition (DDA) samples were run using a linear A–B gradient composed of 3–35% A for 60 min, 35–85% B for 2 min and an isocratic hold at 85% for 5 min, with re-equilibration at 3% A for 7 min. For DDA acquisition, MS1 scans were acquired using a dwell time of 250 ms in the mass range of 400–1,250 *m/z* and the top 50 ions reaching a threshold of 100 counts per second were selected for fragmentation. MS2 scans were acquired in high-sensitivity mode with the dynamic accumulation option turned on with a dwell time of 25 ms for ions ranging from +2 to +5 using rolling collision energy and a collision energy spread of 5. Ions were excluded for fragmentation after one occurrence for a duration of 15 s. Data-independent-acquisition (DIA) files were compared to the DDA library using OpenSWATH as previously outlined⁶⁷. MS2-normalized transition-level data were run through MAP DIA software to obtain normalized peptide and protein level data. In addition, differential protein analysis was performed by MAP DIA⁶⁸. To filter out any peptides that had high variance within triplicates, a coefficient of variation (CV) filter was applied where peptides that had a CV above 20% within each technical replicate were excluded. Peptide-level data were then summed to give protein-level data⁶⁹. These data were then used for downstream analysis, including PCA, GSEA and STRING.

GSEA and STRING analysis. GSEA was conducted as previously described⁷⁰. For matched analysis of mRNA-seq and proteomic data, matching genes found in both datasets were analyzed independently in GSEA. Preranked PC1 gene weightings from each independent PCA were run on the Gene Ontology (GO) and KEGG databases using a GSEA algorithm. Resulting ranked pathway lists from RNA-seq and proteomic analysis were matched using R software and ranked by significance, calculated by false discovery rate (FDR). A predetermined differentially expressed protein list from MAP DIA was used with the STRING protein–protein interaction online tool to give high-confidence protein–protein interactions and enrichments against the whole genome.

MEA recordings. Cells were plated on 48-well MEA plates (Axion Biosystems) at day 15 of differentiation. Spontaneous activity was measured daily for 5 min on the Maestro MEA platform (Axion Biosystems). Waveform events were identified using adaptive spike threshold crossing with an s.d. of electrode noise set at 6, and events were further sorted using Offline Sorter v.4 (Plexon). A minimum of five spikes per minute was used to include events for analysis.

Patch-clamp recordings. Whole-cell patch-clamp recordings were performed on cultures around day 30 that had been plated on L-glass coverslips. Cells were placed in phenol red-free BrainPhys medium (STEMCELL Technologies, 5790) at room temperature and maintained for up to 2 h during acquisition. Glass pipettes were pulled using a Sutter Instruments P-1000 with a tip resistance of 4–5 M Ω . Internal solution comprised 112.5 mM potassium gluconate, 4 mM NaCl, 17.5 mM KCl, 0.5 mM CaCl₂, 1 mM MgCl₂, 5 mM ATP, 1 mM sodium GTP, 5 mM EGTA and 10 mM HEPES. Voltage- and current-clamp recordings were performed using a Multiclamp 700B amplifier, Digidata 1300 and PClamp 10 acquisition software (Molecular Devices). Neurons with an access resistance above 30 M Ω or whose resistance changed more than 4 M Ω during recording were excluded. The resting membrane potential was measured during current clamp by averaging a continuous voltage recording at 0 pA. Voltage-gated sodium and potassium currents were measured from a holding voltage of –70 mV and then stepped from –120 mV to 40 mV in 10-mV increments over 100 ms. Induced action potentials were measured in a current-clamp recording, where the holding current was adjusted to maintain a constant baseline voltage of –60 mV across cells and incrementing steps of 10 pA were applied over 500 ms.

In silico modeling of PKC–PEP005 protein complex. Putative binding of PEP005 to PKC was determined using homology modeling followed by docking studies. Briefly, the C1 domain of PKC δ complexed with 12-acetylphorbol was used as a template (PDB 1PTR)⁷¹. The model structure of PKC α was developed by homology modeling using Rosetta⁷². The top three-dimensional models (out of five predicted structures) of PKC α were then used to assess the binding of PEP005 using Glide⁷³.

The best binding orientation of PEP005 was selected on the basis of Glide XP score. Other putative protein targets for PEP005 were explored using DALI²⁴ on the basis of the three-dimensional structure of the C1 domain of PKC α .

In vivo assessment of PEP005 activity. Wild-type C57BL/6 mice (Jackson Laboratories) were used and all animal work was conducted in accordance with the Institutional Animal Care and Use Committee (6462) at Cedars-Sinai Medical Center. PEP005 was diluted to 10, 1 or 0.1 mM in 0.9% sterile saline solution. Vehicle (DMSO) was diluted to 10 mM in 0.9% sterile saline solution. Mice were given a single 2- μ l injection in the left striatum at the following coordinates: 0.7 mm anteroposterior (AP) and 2.5 mm mediolateral (ML) from bregma and -3.5 mm dorsoventral (DV) from dura. Animals were killed 3 d after injection. For immunohistochemistry analysis, mice were perfused with 4% PFA in PBS and whole brains were extracted and post-fixed in 4% PFA overnight at 4°C. Brains were then rinsed with PBS and stored in 30% sucrose at 4°C. Brains were sectioned at 30 μ m using a microtome and collected as free-floating sections. Striatal sections were washed with PBS three times for 5 min and quenched with 0.3% H₂O₂ for 30 min. Sections were washed with 0.005% Triton X-100 in PBS (PBS-T) three times for 5 min and blocked in a solution of 3% normal horse serum and 2% BSA in PBS-T for 1 h at room temperature, followed by overnight incubation at room temperature in α -synuclein antibody (1:300 dilution, Abcam, ab212184) in blocking solution. The slides were washed with PBS-T three times for 5 min and incubated with biotinylated anti-rabbit IgG (Vector, BA-1000) in blocking solution. Sections were then washed with PBS-T three times for 10 min and incubated for 45 min with Avidin Biotin Complex (Vector, VECTASTAIN ABC Kits (HRP), AK5000), and signal was visualized using DAB (3,3'-diaminobenzidine; 1:500 dilution, Vector, SK4100). For western blot analysis, mice were perfused with PBS and the left and right striatum were dissected. Individual striatal hemispheres were immediately homogenized and lysed in 1 \times NETN buffer supplemented with a phosphatase–protease inhibitor cocktail. Lysates were sonicated by sequential probe followed by bath sonication and centrifuged at 4°C for 20 min at 15,000 r.p.m. Total protein (50 μ g) from each lysate was run on 4–20% Mini-PROTEAN TGX precast gels and transferred to PVDF membranes. Mouse-specific α -synuclein (Abcam, ab212184) and β -actin antibodies were used. Protein bands were quantified by LI-COR software to show relative α -synuclein levels (α -synuclein: β -actin) for the injected relative to the contralateral side.

Reporting Summary. Further information on research design is available in the Nature Research Reporting Summary linked to this article.

Data availability

All requests for raw and analyzed data and materials are promptly reviewed by the Cedars-Sinai Board of Governor's Regenerative Medicine Institute to verify whether the request is subject to any intellectual property or confidentiality obligations. Patient-related data not included in the paper may be subject to patient confidentiality. Any data and materials that can be shared will be released via a material transfer agreement. All transcriptomic data from this study are available in the GEO repository under GSE120746. The mass spectrometry proteomics data have been deposited to the ProteomeXchange Consortium with the dataset identifier PXD011326.

References

- Barrett, R. et al. Reliable generation of induced pluripotent stem cells from human lymphoblastoid cell lines. *Stem Cell Transl. Med.* **3**, 1429–1434 (2014).
- Mazzulli, J. R. et al. Gaucher disease glucocerebrosidase and α -synuclein form a bidirectional pathogenic loop in synucleinopathies. *Cell* **146**, 37–52 (2011).
- Marshall, J. et al. Demonstration of feasibility of in vivo gene therapy for gaucher disease using a chemically induced mouse model. *Mol. Ther.* **6**, 179–189 (2002).
- Ho, R. et al. ALS disrupts spinal motor neuron maturation and aging pathways within gene co-expression networks. *Nat. Neurosci.* **19**, 1256–1267 (2016).
- Dobin, A. et al. STAR: ultrafast universal RNA-seq aligner. *Bioinformatics* **29**, 15–21 (2013).

- Li, B. & Dewey, C. N. RSEM: accurate transcript quantification from RNA-seq data with or without a reference genome. *BMC Bioinforma.* **12**, 323 (2011).
- Schubert, O. T. et al. Building high-quality assay libraries for targeted analysis of SWATH MS data. *Nat. Protoc.* **10**, 426–441 (2015).
- Teo, G. et al. mapDIA: preprocessing and statistical analysis of quantitative proteomics data from data-independent acquisition mass spectrometry. *J. Proteom.* **129**, 108–120 (2015).
- Parker, S. J., Venkatraman, V. & Van Eyk, J. E. Effect of peptide assay library size and composition in targeted data-independent acquisition-MS analyses. *Proteomics* **16**, 2221–2237 (2016).
- Subramanian, A. et al. Gene-set enrichment analysis: a knowledge-based approach for interpreting genome-wide expression profiles. *Proc. Natl Acad. Sci. USA* **102**, 15545–15550 (2005).
- Zhang, G., Kazanietz, M. G., Blumberg, P. M. & Hurley, J. H. Crystal structure of the cys2 activator-binding domain of protein kinase C in complex with phorbol ester. *Cell* **81**, 917–924 (1995).
- Kim, D. E., Chivian, D. & Baker, D. Protein structure prediction and analysis using the Robetta server. *Nucleic Acids Res.* **32**, W526–W531 (2004).
- Morin, A. et al. Collaboration gets the most out of software. *eLife* **2**, e01456 (2013).
- Holm, L., Kaariainen, S., Wilton, C. & Plewczynski, D. Using Dali for structural comparison of proteins. *Curr. Protoc. Bioinformatics* **Chapter 5**, 5 (2006).

Acknowledgements

We thank S. Svendsen for critical input and editing of the manuscript and T. Pierson for consultation on protein degradation and additional editing of the manuscript. We also thank A. Singleton and D. Hernandez for NeuroX analysis and WGS of patient samples, R. Holewinski for assistance with proteomic analysis and sample acquisition, V. Mattis and H. Park for assisting with striatal dissections, D. Torolina for sectioning and staining of mouse brains and G. Lawless for assistance with ELISA assays. We also thank the Cedars-Sinai Proteomics and Metabolomics Core. The majority of this work was supported by the Joseph Drown Foundation (C.N.S.) and the Board of Governors Regenerative Medicine Institute (C.N.S.) and a National Institutes of Health grant, 5UG3NS105703-02 (C.N.S.). Support for the clinical sample collection and patient information came from the Widjaja Family Foundation (M.T.). Support for the proteomics analysis was from the Advanced Clinical Biosystems Institute (J.E.V.E.).

Author contributions

A.H.L., S.S., N.Y. and C.N.S. designed experiments. A.H.L., S.S., N.Y., V.J.D., V.J.G. and A.N.F. performed experiments. A.H.L., S.S. and C.N.S. wrote the manuscript. S.S. and R.H. performed transcriptomic analysis. P.A. performed all animal work and K.M.R. processed brain tissue. S.S., A.H.L., D.W. and M.G.B. generated YOPD iPSC lines. R.M. performed in silico modeling. M.R.J. performed WGS analysis. Z.S. and N.T.M. performed dopamine release experiments. J.E.V.E. supervised the proteomic data analysis. M.T. provided patient samples and clinical data, and helped supervise the project. C.N.S. supervised the project.

Competing interests

An intellectual protection patent is pending for diagnostic and drug screening for molecular signatures of early-onset sporadic Parkinson's disease.

Additional information

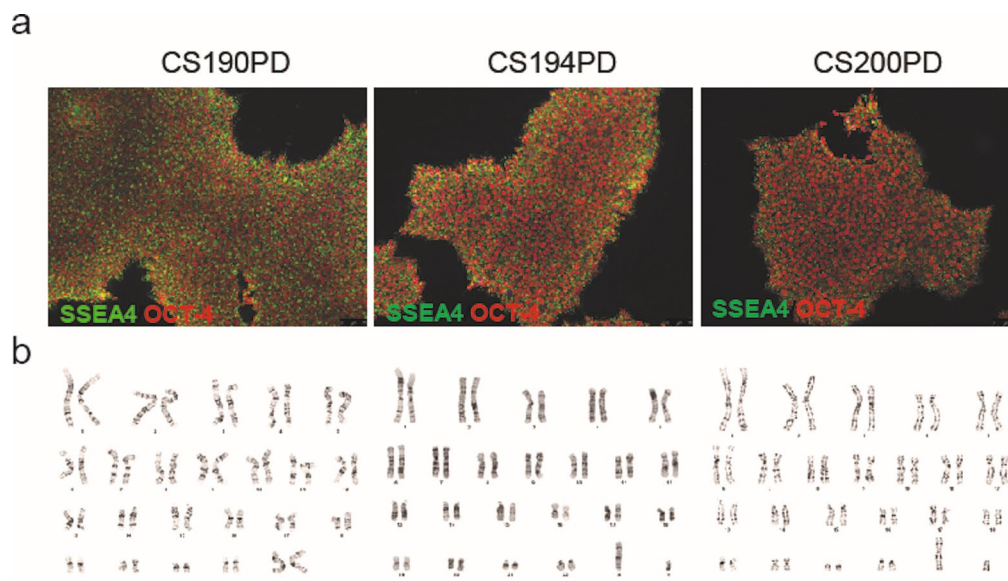
Extended data is available for this paper at <https://doi.org/10.1038/s41591-019-0739-1>.

Supplementary information is available for this paper at <https://doi.org/10.1038/s41591-019-0739-1>.

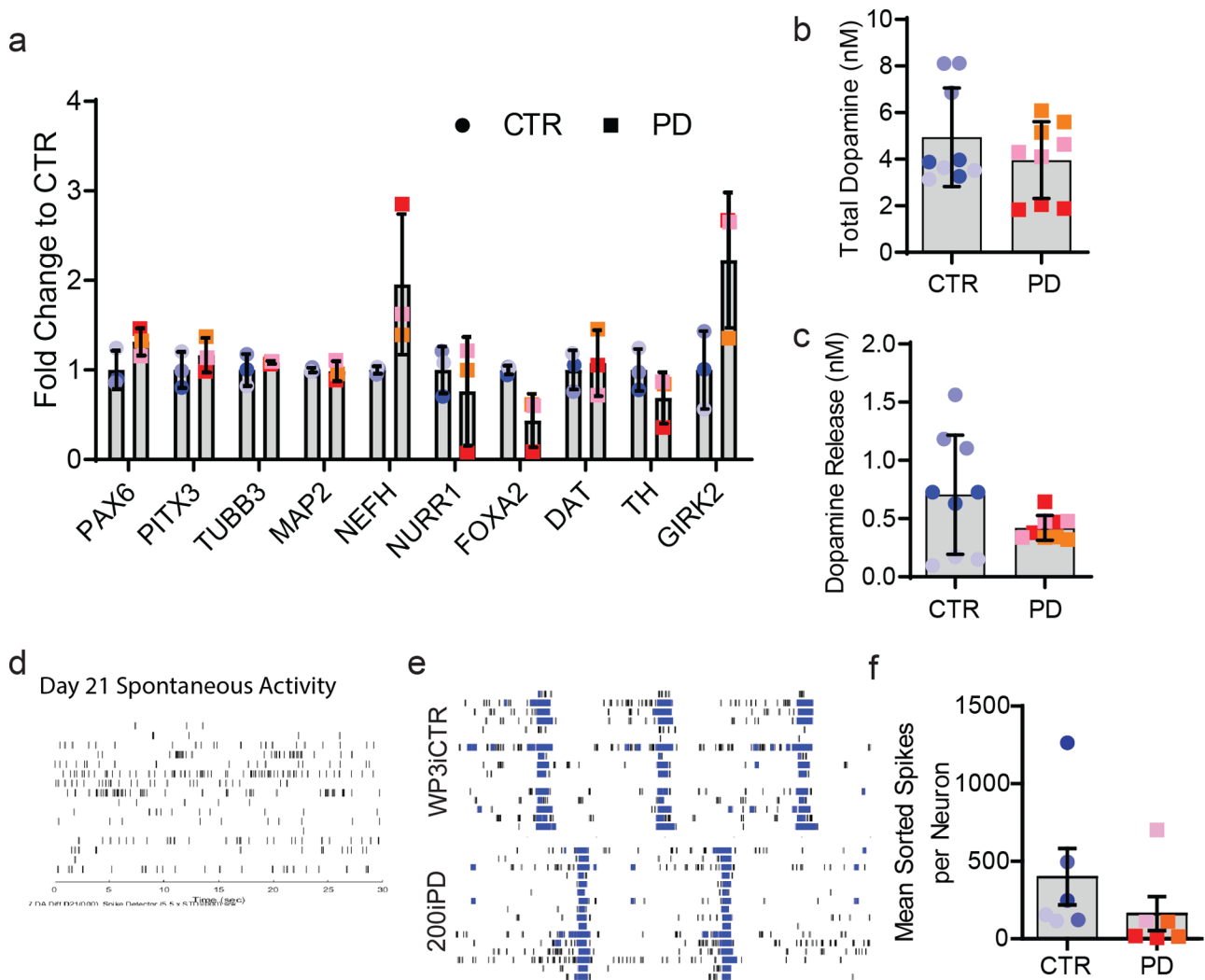
Correspondence and requests for materials should be addressed to C.N.S.

Peer review information Brett Benedetti and Kate Gao were the primary editors on this article and managed its editorial process and peer review in collaboration with the rest of the editorial team.

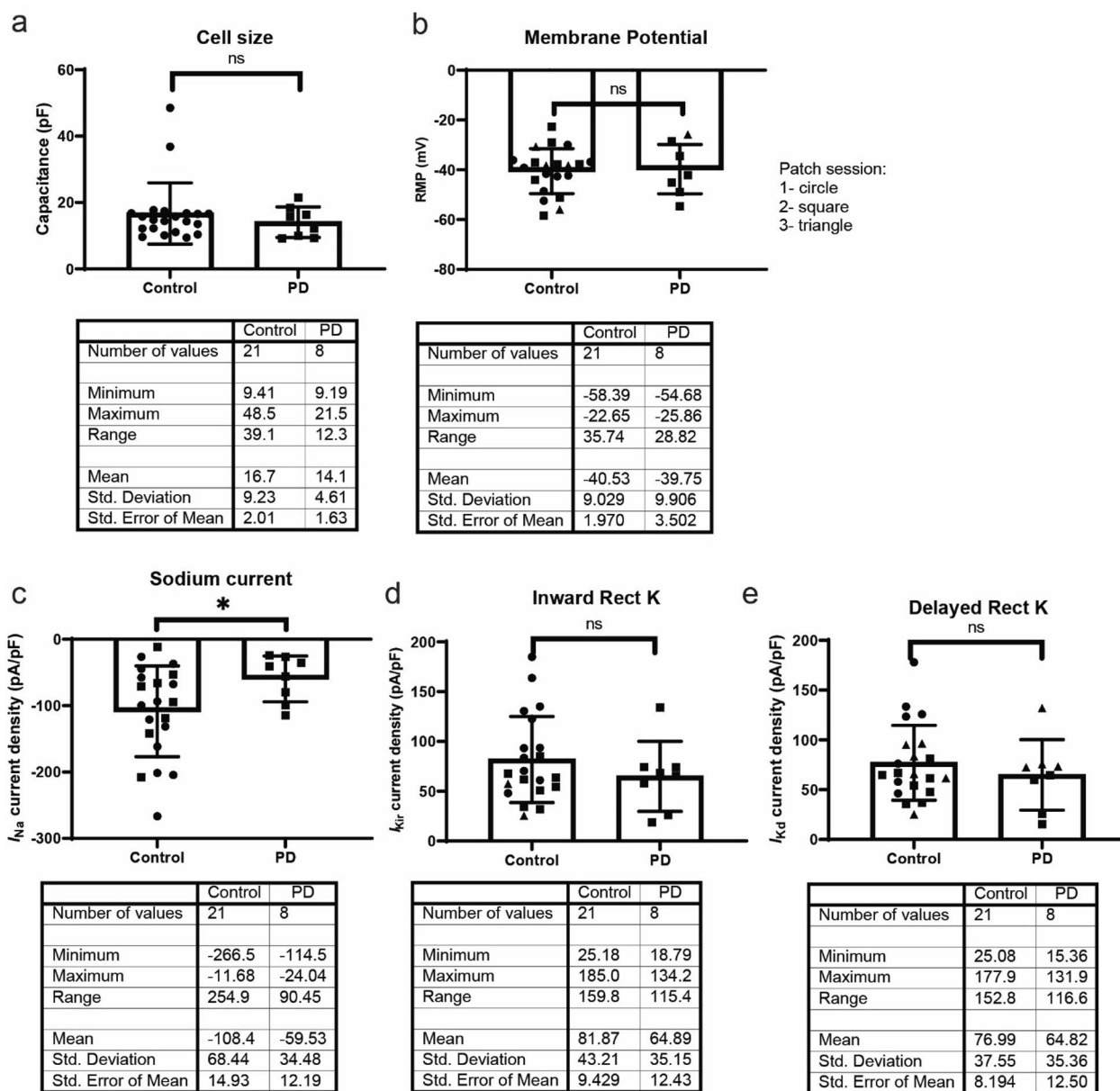
Reprints and permissions information is available at www.nature.com/reprints.



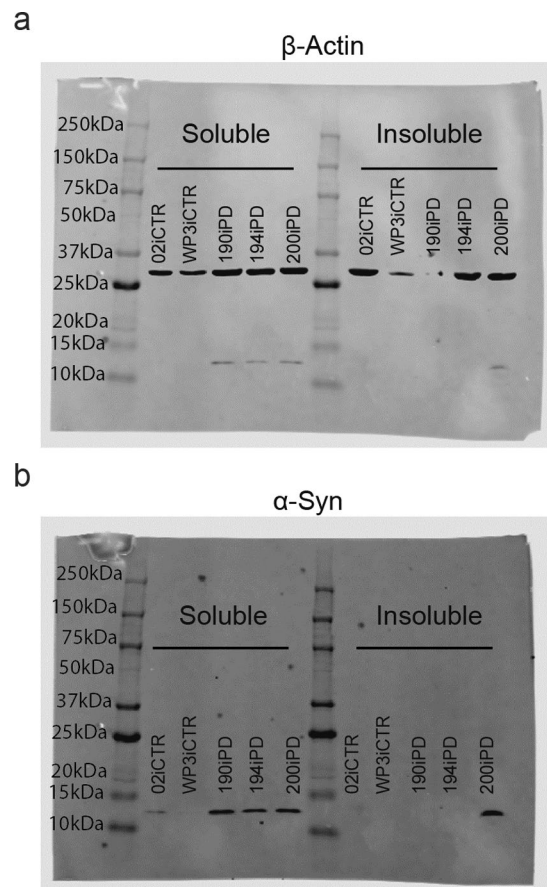
Extended Data Fig. 1 | Generation of YOPD iPSCs. (a) SSEA4 (green) and OCT-4 immunostaining in undifferentiated iPSCs from YOPD patients. **(b)** Normal karyotypes from YOPD patient iPSCs, 20 metaphase spreads were analyzed for each line.



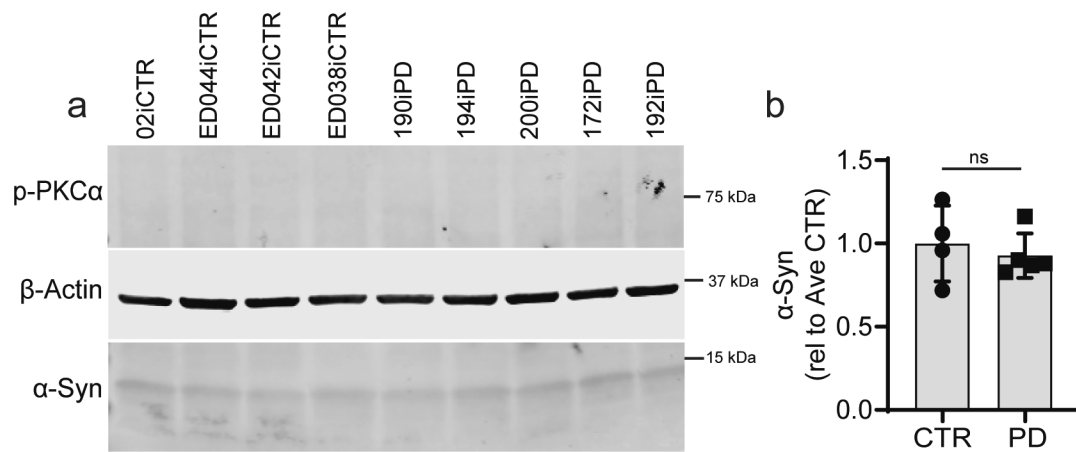
Extended Data Fig. 2 | Additional characterization of mDA cultures. (a) Expression of dopaminergic neuron genes in day 30 mDA cultures from 6 iPSC lines. 3 biological replicates per line were averaged. Data are normalized to average expression in control lines and presented as 3 CTR vs 3 PD lines. No significant differences were detected using multiple t-tests with Holm-Sidak correction for multiple comparisons. (b) HPLC detection of total dopamine in d30 mDA culture lysates. $n=9$ CTR $n=9$ PD not significant $p=0.29$ two-tailed t-test with Welch's correction. (c) HPLC detection of released dopamine in aCSF following a 15 min incubation at 37°C . $n=9$ CTR $n=9$ not significant $p=0.14$ two-tailed t-test with Welch's correction. (d) MEA recording of spontaneous activity from O2iCTR mDA neurons at day 21 of differentiation. (e) MEA recordings of control and YOPD mDA neurons at d30 of differentiation. (f) Average sorted spikes per neuron at d30. Points represent an average of 4 independent wells, $n=6$ CTR $n=6$ PD colors indicate iPSC lines. Bar graphs represent mean, error bars represent standard deviation (s.d.).



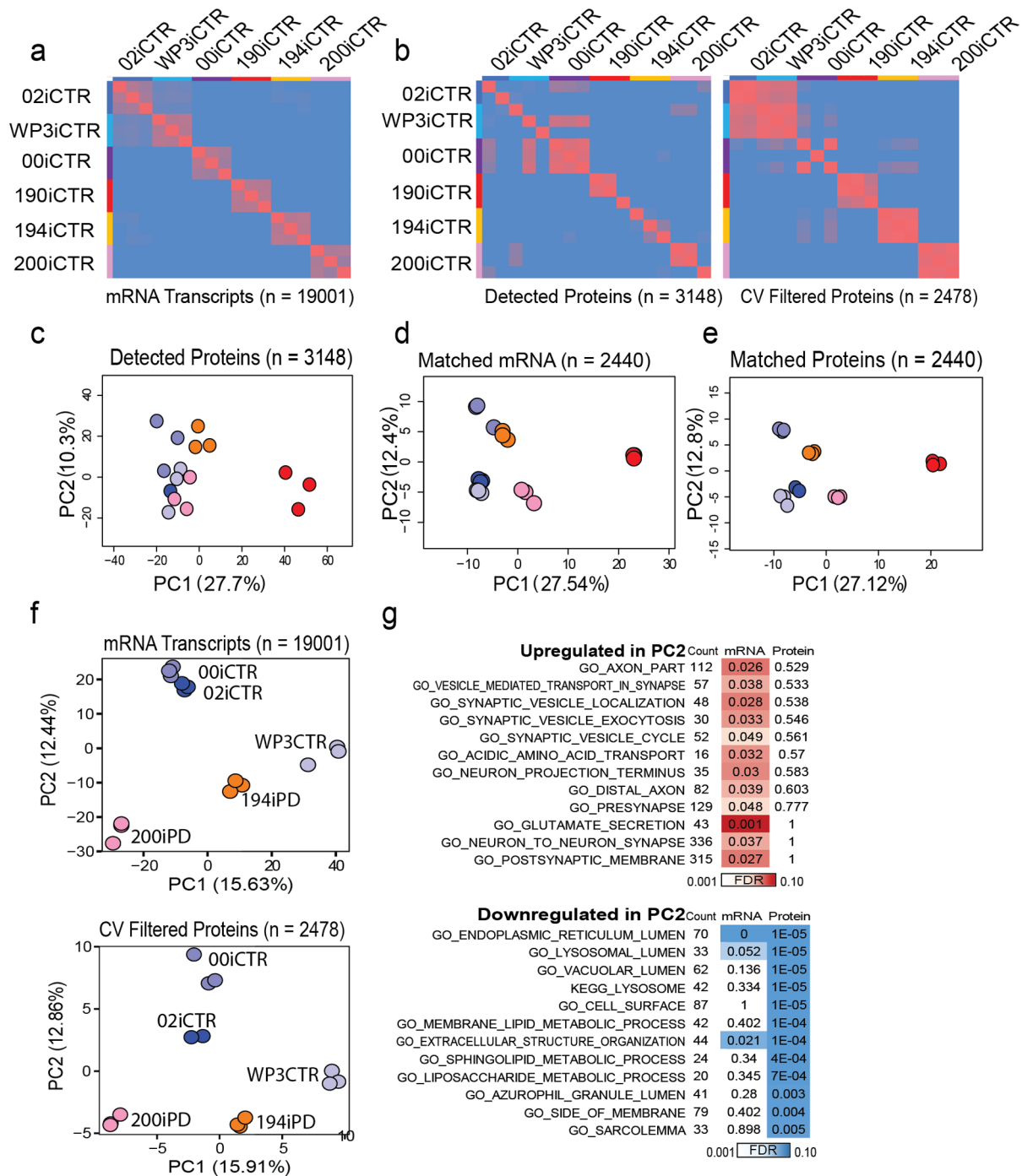
Extended Data Fig. 3 | Whole-cell patch clamp measurements from control and YOPD mDA cultures. (a) Capacitance is similar between control and YOPD. (b) No difference in resting membrane potential (RMP) is observed. (c) Voltage-gated sodium current density is decreased in YOPD compared to control. No difference is observed in either the (d) inwards rectifying potassium current density, or (e) delayed rectifier potassium current density. * denotes significance $p = 0.018$ two tailed t-test with Welch's correction. Bar graphs represent mean, error bars represent standard deviation (s.d.).



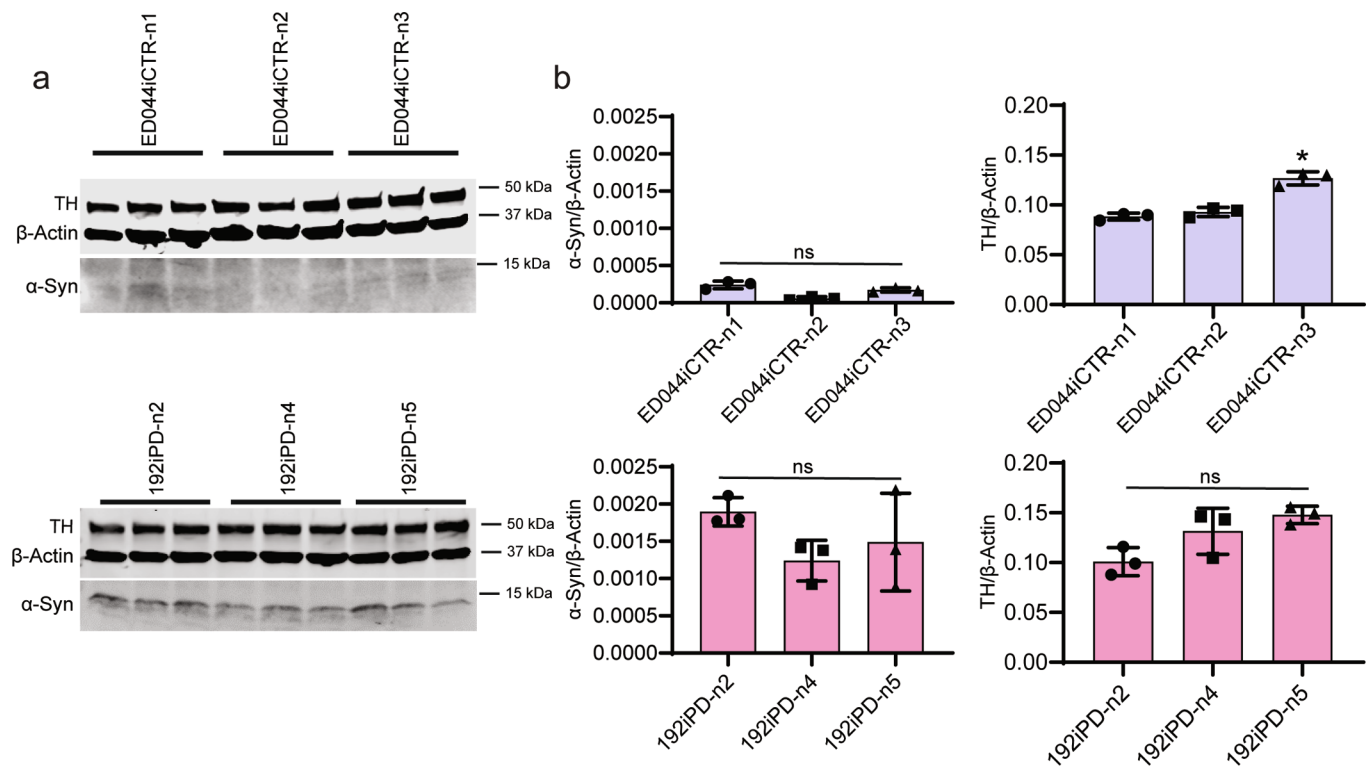
Extended Data Fig. 4 | Western blots of soluble and insoluble lysate fractions. Western blot of D30 mDA cultures under non-denaturing conditions for α -synuclein and loading control of β -actin. Fractionation experiment was conducted once in 5 independent iPSC lines.



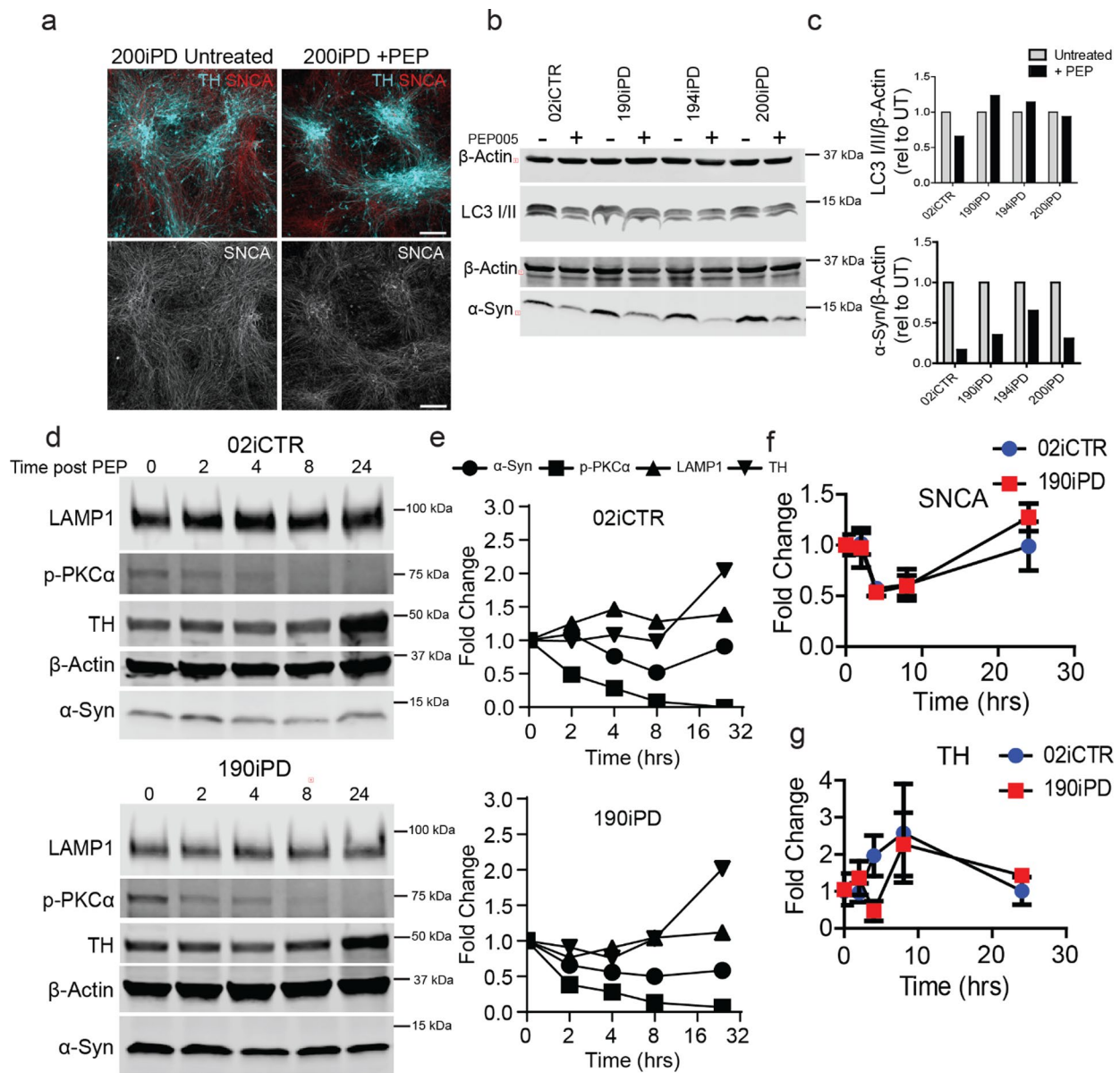
Extended Data Fig. 5 | Western blots of YOPD markers in undifferentiated iPSCs. (a) Western blot of p-PKC α and α -Syn in undifferentiated iPSCs and **(b)** relative quantification of α -Syn levels ($n=4$ CTR $n=5$ PD $p=0.87$ two-tailed t-test with Welch's correction); no quantification of p-PKC α was possible in the iPSCs as no bands were detected. Bar graphs represent mean, error bars represent standard deviation (s.d.).



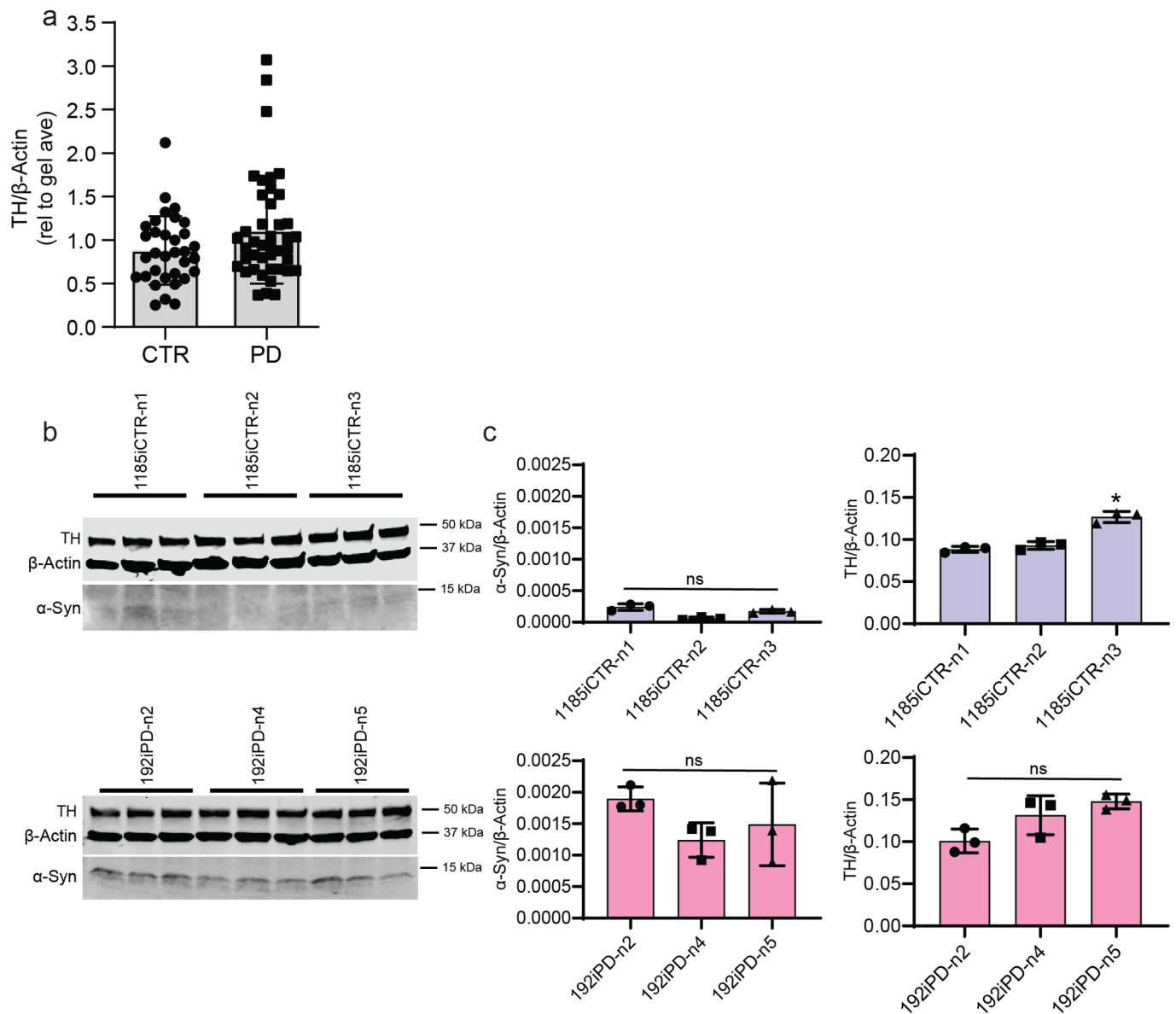
Extended Data Fig. 6 | Paired transcriptomic and proteomic analysis. Pearson correlation plots of (a) transcriptomic and (b) proteomic data. (c) PCA plot of all detected proteins. (d) PCA plot of matching RNA-Seq transcripts. (e) PCA plot of matching proteins. (f) PCA plots of filtered data with 190iPD line omitted. (g) Matched GSEA terms conducted on 190iPD omitted data set n=9 CTR n=6 PD term significance determined by FDR <0.1.



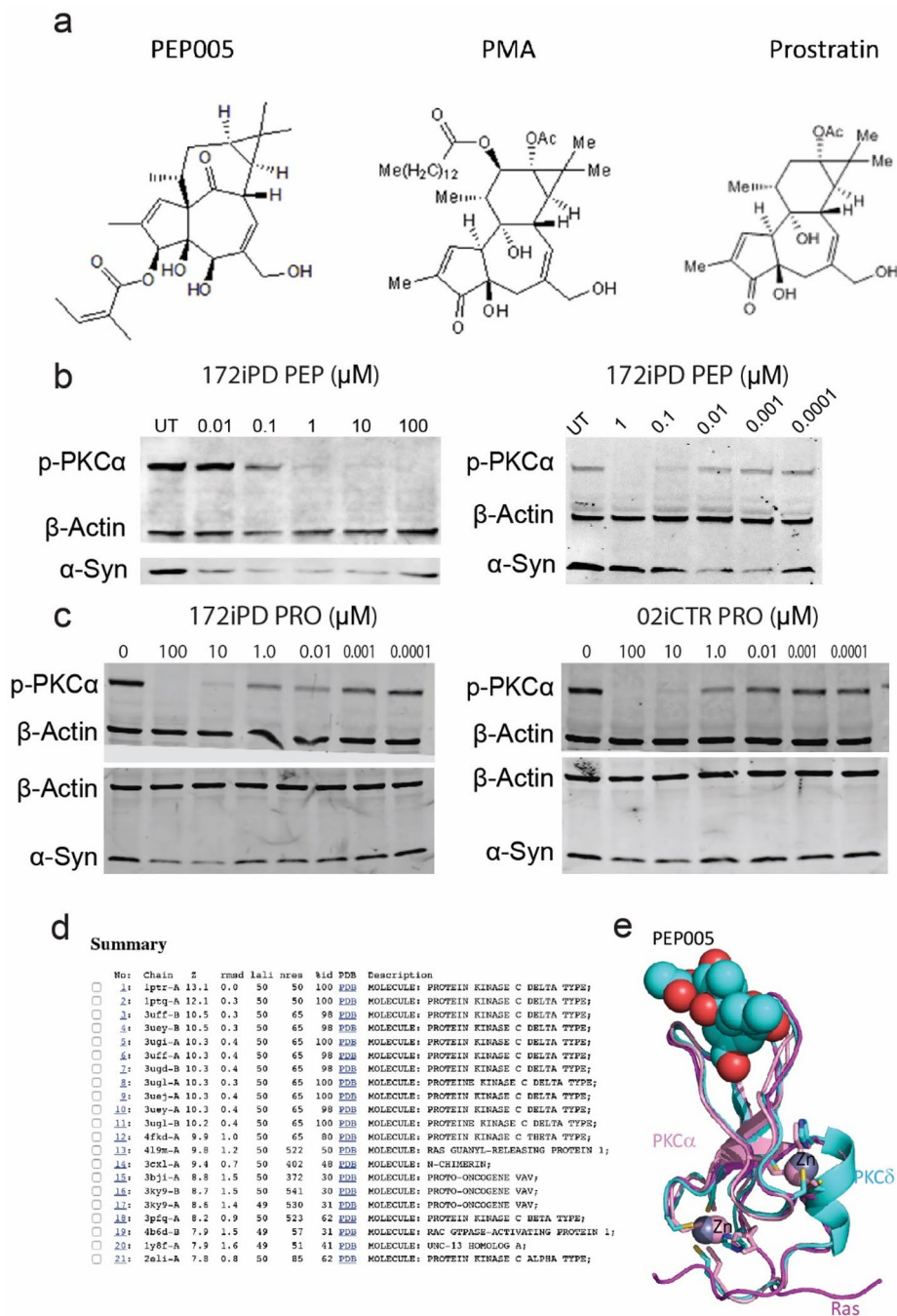
Extended Data Fig. 7 | Testing of additional Proteasomal inhibitors. (a) Western blot of D30 mDA cultures in the presence of indicated proteasomal inhibitors. Quantification of blots from multiple differentiations ($n=4$ CTR, $n=4$ PD) with each point representing a band intensity from a separate differentiation. (b) P53 one-way ANOVA with Tukey multiple comparisons test ($F 17.53$ DF 20 $p=0.0005$ CTR Lac $p=0.0003$ CTR Epox $p=0.0009$ PD Lac $p=0.001$ PD Epox). (c) α -Syn one-way ANOVA with Tukey multiple comparisons test ($F 1.6$ DF 20 $p=0.0.21$). Bar graphs represent mean, error bars represent standard deviation (s.d.).



Extended Data Fig. 8 | Additional characterization of PEP005 treatment. (a) Immunocytochemistry showing TH and α -synuclein (α -Syn) in 200iPD d30 mDA cultures with and without PEP005 treatment. Images are representative of 2 additional lines tested. (b) Day 30 mDA neurons treated with PEP005 from multiple YOPD and control lines. (c) Quantification of LC3I/II and α -Syn band intensities relative to untreated cells from the same line. (d) Time-course of PEP005 treatment in YOPD and control mDA neurons. (e) Quantification of α -Syn, p-PKC α , LAMP1, and TH band intensities in YOPD and control mDA neurons in timecourse study. qPCR from paired samples (n=3 wells 02iCTR n=3 wells 190iPD) over PEP005 time-course showing (f) SNCA and (g) TH expression. Bar graphs represent mean, error bars represent standard deviation (s.d.).



Extended Data Fig. 9 | mDA differentiation across multiple lines and clones. (a) Tyrosine Hydroxylase (TH) production by western blot across 8 control and 12 YOPD patients. TH levels were first normalized to β -actin, then to compare across blots the levels were normalized to the average signal (TH/ β -actin) of each gel. (b) Western blots of TH and α -synuclein (α -Syn) levels in day 30 mDA cultures across 3 unique clonal lines from ED044iCTR and from 192iPD. (c) Quantification of band intensities for TH and α -Syn normalized to β -actin. Bands represent independent biological replicates from 3 separate wells differentiated in the same experiment. *indicates $p=0.0002$ via one-way ANOVA (F 51.42, DF 8) with Tukey multiple comparisons test compared to other clones of the same line. Bar graphs represent mean, error bars represent standard deviation (s.d.).



Extended Data Fig. 10 | Dose-response and *in silico* analysis of PEP005 and related molecules. (a) Structures of Phorbol esters similar to PEP005 tested in mDA cultures. **(b)** Western blots of α -synuclein (α -Syn) and p-PKC α in response to varying PEP005 doses. **(c)** Western blots of α -Syn and p-PKC α in response to varying Prostratin (PRO) doses in both YOPD and control mDA cultures. Dose ranging studies were repeated twice. **(d)** Predictive modeling of PEP005 binding sites on PKC α and similar affinity sites on additional proteins. **(e)** Three dimensional model of PEP005 binding sites on PKC α , PKC δ , and Ras overlaid to show similarity.

Reporting Summary

Nature Research wishes to improve the reproducibility of the work that we publish. This form provides structure for consistency and transparency in reporting. For further information on Nature Research policies, see [Authors & Referees](#) and the [Editorial Policy Checklist](#).

Statistics

For all statistical analyses, confirm that the following items are present in the figure legend, table legend, main text, or Methods section.

n/a Confirmed

- The exact sample size (n) for each experimental group/condition, given as a discrete number and unit of measurement
- A statement on whether measurements were taken from distinct samples or whether the same sample was measured repeatedly
- The statistical test(s) used AND whether they are one- or two-sided
Only common tests should be described solely by name; describe more complex techniques in the Methods section.
- A description of all covariates tested
- A description of any assumptions or corrections, such as tests of normality and adjustment for multiple comparisons
- A full description of the statistical parameters including central tendency (e.g. means) or other basic estimates (e.g. regression coefficient) AND variation (e.g. standard deviation) or associated estimates of uncertainty (e.g. confidence intervals)
- For null hypothesis testing, the test statistic (e.g. F , t , r) with confidence intervals, effect sizes, degrees of freedom and P value noted
Give P values as exact values whenever suitable.
- For Bayesian analysis, information on the choice of priors and Markov chain Monte Carlo settings
- For hierarchical and complex designs, identification of the appropriate level for tests and full reporting of outcomes
- Estimates of effect sizes (e.g. Cohen's d , Pearson's r), indicating how they were calculated

Our web collection on [statistics for biologists](#) contains articles on many of the points above.

Software and code

Policy information about [availability of computer code](#)

Data collection

BD FACSDiva v8.0.1 was used to collect and analyze flow data.

Data analysis

Raw reads obtained from RNA-Seq were aligned to the transcriptome using STAR (version 2.5.0)⁶¹ / RSEM (version 1.2.25)⁶² with default parameters, using a custom human GRCh38 (or mouse CRCm38) transcriptome reference downloaded from <http://www.encodegenes.org>, containing all protein coding and long non-coding RNA genes based on human GENCODE version 23 (or Mouse GENCODE M8) annotation. Expression counts for each gene (TPM: transcripts per million) in all samples were normalized by the sequencing depth. To determine detected transcripts, a filter of >0.1TPM in at least 9 samples was used as a threshold for detection of a unique transcript (Cluster 3.0). PCA was conducted on log transformed data using Cluster 3.0 software. Gene set enrichment analysis (GSEA) was conducted as previously described⁶⁶. For matched analysis of mRNA-Seq and proteomic data, matching genes found in both data sets were analyzed independently in GSEA. Preranked PC1 gene weightings from each independent PCA analysis were run on Gene Ontology (GO) and KEGG databases using GSEA algorithm. Resulting ranked pathway lists from RNA-Seq and proteomic analysis were matched using R software and ranked by significance calculated by FDR. Predetermined differentially expressed protein list from MAP DIA was used with STRING protein:protein interaction online tool to give high confidence protein:protein interactions and enrichments against the whole genome. Graphpad Prism 8 was used to create graphs and conduct statistical analysis. IMARIS software v9.1 (bitplane) was used to visualize ICC images

For manuscripts utilizing custom algorithms or software that are central to the research but not yet described in published literature, software must be made available to editors/reviewers. We strongly encourage code deposition in a community repository (e.g. GitHub). See the Nature Research [guidelines for submitting code & software](#) for further information.

Data

Policy information about [availability of data](#)

All manuscripts must include a [data availability statement](#). This statement should provide the following information, where applicable:

- Accession codes, unique identifiers, or web links for publicly available datasets
- A list of figures that have associated raw data
- A description of any restrictions on data availability

All requests for raw and analyzed data and materials are promptly reviewed by the Cedars-Sinai Board of Governor's Regenerative Medicine Institute to verify if the request is subject to any intellectual property or confidentiality obligations. Patient-related data not included in the paper may be subject to patient confidentiality. Any data and materials that can be shared will be released via a Material Transfer Agreement. All transcriptomic data from this study is available in the GEO repository under GSE120746. The mass spectrometry proteomics data have been deposited to the ProteomeXchange Consortium with the dataset identifier PXD011326.

Field-specific reporting

Please select the one below that is the best fit for your research. If you are not sure, read the appropriate sections before making your selection.

- Life sciences Behavioural & social sciences Ecological, evolutionary & environmental sciences

For a reference copy of the document with all sections, see [nature.com/documents/nr-reporting-summary-flat.pdf](https://www.nature.com/documents/nr-reporting-summary-flat.pdf)

Life sciences study design

All studies must disclose on these points even when the disclosure is negative.

Sample size	From our initial cohort of 3 ctrl and 3 PD patients a power analysis (t-test two tails effect size 1.94 alpha 0.05 power 0.95) determined that 8 individuals per group were necessary. Our full cohort contained 10 control and 12 YOPD patients.
Data exclusions	Data from some differentiations was excluded from this study because the originating iPSC lines were outside of our pre-established range between passages p17-p35. This range was established because iPSCs maintained in E8 past p40 lost the ability to efficiently differentiate to TH expressing neurons.
Replication	All experiments were repeated from at least 3 independent differentiations and all attempts at replication were successful. Except where noted in figure legends 3 biological replicates were averaged for each experiment and presented as a single point.
Randomization	All samples from EOSPD and control cells were differentiated and analyzed together in each experiment.
Blinding	Investigators were blinded to group allocation during data collection for initial detection of YOPD biomarkers by western blot. Blinding for remaining experiments was not possible due to the identification of cell line GUIDs from expanded cohorts.

Reporting for specific materials, systems and methods

We require information from authors about some types of materials, experimental systems and methods used in many studies. Here, indicate whether each material, system or method listed is relevant to your study. If you are not sure if a list item applies to your research, read the appropriate section before selecting a response.

Materials & experimental systems

n/a	Involved in the study
<input type="checkbox"/>	<input checked="" type="checkbox"/> Antibodies
<input type="checkbox"/>	<input checked="" type="checkbox"/> Eukaryotic cell lines
<input checked="" type="checkbox"/>	<input type="checkbox"/> Palaeontology
<input type="checkbox"/>	<input checked="" type="checkbox"/> Animals and other organisms
<input type="checkbox"/>	<input checked="" type="checkbox"/> Human research participants
<input checked="" type="checkbox"/>	<input type="checkbox"/> Clinical data

Methods

n/a	Involved in the study
<input checked="" type="checkbox"/>	<input type="checkbox"/> ChIP-seq
<input type="checkbox"/>	<input checked="" type="checkbox"/> Flow cytometry
<input checked="" type="checkbox"/>	<input type="checkbox"/> MRI-based neuroimaging

Antibodies

Antibodies used

human α -synuclein (1:1000, Abcam #ab138501), mouse α -synuclein (1:1000, Abcam # ab212184), TH (1:2000, ImmunoStar, # 22941), total PKC α (1:1000, Cell Signaling, #2056S), p-PKC α 1:1000, Cell Signaling, # 9375s), LAMP1(1:1000, Cell Signaling, #9091S), LCI/II (1:1000, Cell Signaling, #12741S clone D3U4C), Cleaved Caspase 3-CC3(1:1000, Cell Signaling #9661S), Synaptophysin (1:1000, Abcam, ab32127 clone YE269), P53 (1:2000, Santa Cruz, #sc-126 clone DO-1), GAPDH (1:5000, Sigma-Aldrich, G8795 clone GAPDH-71.1) and β -actin (1:5000, Sigma-Aldrich, #A5441 clone AC-15)

Validation

All antibodies were selected based on validation statements on the manufacturer's website for reactivity to the protein and species specified by the manufacturer. Anti TH (ImmunoStar # 22941) was selected from its use in Kriks, S., et al. Dopamine neurons derived from human ES cells efficiently engraft in animal models of Parkinson's disease. Nature 480, 547-551 (2011).

Eukaryotic cell lines

Policy information about [cell lines](#)

Cell line source(s)

All iPSC lines used in this study were derived by the Cedars-Sinai iPSC core

Authentication

All iPSC lines were tested for Karyotype, expression of pluripotency markers (SSEA4, OCT4, TRA1, NANOG, SOX2), and hPSC scorecard assay

Mycoplasma contamination

All cells were negative for mycoplasma. Testing was performed on a bi-monthly basis throughout the course of the study.

Commonly misidentified lines
(See [ICLAC](#) register)

No commonly misidentified lines were used in this study

Animals and other organisms

Policy information about [studies involving animals](#); [ARRIVE guidelines](#) recommended for reporting animal research

Laboratory animals

Male WT C57BL/6 mice age 70 days were purchased from Jackson labs

Wild animals

This study did not involve wild animals

Field-collected samples

This study did not involve field-collected samples

Ethics oversight

All mice work in this study was performed under guidelines of the Cedars-Sinai Medical Center Institutional Animal Care and Use Committee (IACUC) under protocol #6462.

Note that full information on the approval of the study protocol must also be provided in the manuscript.

Human research participants

Policy information about [studies involving human research participants](#)

Population characteristics

All patients participating in this study were selected solely for the diagnosis of YOPD (diagnosis between 21 and 50 YOA). Gender, language, or ethnicity were not considered.

Recruitment

Patients were selected from either the AMP-PD database through the PDBP program or through the Cedars-Sinai Movement Disorders clinic. Potential candidates at Cedars with early onset PD and no family history were asked if they were interested in participating in this study under appropriate IRB controls. We are not aware of any specific bias's in our patient population.

Ethics oversight

All the cell lines and protocols in the present study were used in accordance with the guidelines approved by the stem cell research oversight committee (SCRO) and institutional review board (IRB) under the auspice IRB-SCRO Protocols Pro00032834 (iPSC Core Repository and Stem Cell Program), Pro00021505 (Svendsen Stem Cell Program).

Note that full information on the approval of the study protocol must also be provided in the manuscript.

Flow Cytometry

Plots

Confirm that:

- The axis labels state the marker and fluorochrome used (e.g. CD4-FITC).
- The axis scales are clearly visible. Include numbers along axes only for bottom left plot of group (a 'group' is an analysis of identical markers).
- All plots are contour plots with outliers or pseudocolor plots.
- A numerical value for number of cells or percentage (with statistics) is provided.

Methodology

Sample preparation

Day-30 cultures in 6-well plates were washed once in phosphate buffered saline (PBS) then 1mL Accutase was added to each well and incubated for 25 mins at 37°C or until the cells fully lifted. Cells were washed with an additional 2mL Maturation Medium and very gently triturated until large clumps were no longer visible at which point cells were pelleted by centrifugation (1500 RPM for 3 mins). Cells were gently resuspended in 4% paraformaldehyde (PFA) in PBS and allowed to fix for 10-15 mins at room temperature. Fixed single cells were permeabilized using 1% Triton X-100 (Sigma-Aldrich) and stained using primary antibodies against TH (1:500 Immunostar, 22941), α -synuclein (1:1000 Abcam, ab138501), and MAP2ab (1:1000 Sigma-Aldrich, M1406), or isotype controls at same dilution (Cell Signaling IgG Isotype Control rabbit #3900S and mouse #5415S). Secondary

antibodies (Alexa Fluor 488 and 594 donkey anti-mouse and donkey anti-rabbit, Invitrogen) were used at 1:500. Stained samples were quantified on an LSR Fortessa cytometer using BD FACSDiva software.

Instrument

BD LSR Fortessa

Software

BD FACSDiva software

Cell population abundance

We sorted 20k events per sample. We then gated roughly 35% of all events as cells and ~20% of all cells were TH positive

Gating strategy

Initial FSC/SSC gates were determined from contour plots. Positive TH expressing cells (FITC channel) were identified against a sample stained with an isotype control antibody.

Tick this box to confirm that a figure exemplifying the gating strategy is provided in the Supplementary Information.